LETTER

KLHL22 activates amino–acid–dependent mTORC1 signalling to promote tumorigenesis and ageing

Jie Chen[1,2], Yuhui Ou[1], Yanyan Yang[1], Wen Li[3], Ye Xu[4], Yuntao Xie[4] & Ying Liu[1]*

The mechanistic target of rapamycin complex 1 (mTORC1) is a master regulator of cell growth that responds to a diverse set of environmental cues, including amino acids[1,2]. Deregulation of mTORC1 has been linked with metabolic diseases, cancer and ageing[2–4]. In response to amino acids, mTORC1 is recruited by the Rag GTPases to the lysosome, its site of activation[5,6]. The GATOR1 complex, consisting of DEPDC5, NPRL3 and NPRL2, displays GAP activity to inactivate Rag GTPases under amino-acid-deficient conditions[7]. However, it is unclear how the inhibitory function of GATOR1 is released upon amino acid stimulation. Here we find that in response to amino acids, the CUL3–KLHL22 E3 ubiquitin ligase promotes K48-linked polyubiquitination and degradation of DEPDC5, an essential subunit of GATOR1. KLHL22 plays a conserved role to mediate the activation of mTORC1 and downstream events in mammals and nematodes. Depletion of MEL-26, the *Caenorhabditis elegans* orthologue of KLHL22, extends worm lifespan. Moreover, KLHL22 levels are elevated in tumours of breast cancer patients, whereas DEPDC5 levels are correspondingly reduced. Depletion of KLHL22 in breast cancer cells suppresses tumour growth in nude mice. Therefore, pharmacological interventions targeting KLHL22 may have therapeutic potential for the treatment of breast cancer and age-related diseases.

To understand how inhibition by GATOR1 is released during mTORC1 activation, we monitored the stability of GATOR1 subunits in response to amino acid availability. Notably, the protein levels of DEPDC5, but not NPRL3 or NPRL2, were regulated in an amino-acid-sensitive manner (Fig. 1a and Extended Data Fig. 1a). By contrast, levels of DEPDC5 transcripts remained unchanged in the presence or absence of amino acids (Extended Data Fig. 1b). The stability of DEPDC5 protein was extremely low under the basal culturing condition (Extended Data Fig. 1c, d). Accumulation of DEPDC5 was detected only when we treated cells with MG132, the 26S proteasome inhibitor (Extended Data Fig. 1e), suggesting that DEPDC5 undergoes proteasome-mediated degradation in response to amino acids.

Covalent conjugation of ubiquitin is a key step in proteasome-mediated degradation of target proteins. Indeed, the ubiquitination of DEPDC5 was observed in the presence of amino acids (Fig. 1b and Extended Data Fig. 1f). DEPDC5 could be labelled only with wild-type or K48 ubiquitin (ubiquitin mutant that contains only one lysine), but not with K63 ubiquitin (Fig. 1c), indicating that amino acids promote K48-linked ubiquitination of DEPDC5.

We next sought to identify the E3 ubiquitin ligase that targets DEPDC5. Because mTORC1 signalling is often deregulated in human cancers[8,9], and the GATOR1 complex has been reported to function on the lysosomal surface[10], we screened a panel of E3 ligases that have been reported to affect mTORC1 activity or tumorigenesis, together with E3 ligases localized to the lysosomes. We found that ectopic expression of KLHL22, mutations of which have been linked with breast cancer[11], promoted the degradation of endogenous DEPDC5 (Extended Data Fig. 2a). KLHL22 is a BTB (Bric-á-brac–Tramtrack–Broad) adaptor

protein, usually forming a functional cullin–RING E3 ubiquitin ligase complex with the scaffold protein CUL3 and the ring-finger protein RBX1[12,13]. Notably, CUL3 and RBX1 were identified by mass spectrometry during our search for DEPDC5-interacting proteins (Extended Data Fig. 2b). The substrate specificity of cullin–RING E3 ubiquitin ligase is determined through a BTB adaptor protein within the complex[14]. Indeed, overexpression of CUL3–RBX1–KLHL22, but not CUL3–RBX1–KLHL19, promoted the ubiquitination and degradation of DEPDC5 (Fig. 1d, e). Deletion of the 6-Kelch (6K) repeats, the substrate recognition motif of KLHL22[15], or knockdown of *KLHL22* by small interfering RNA (siRNA), blocked DEPDC5 ubiquitination and degradation (Fig. 1d–g). Furthermore, recombinant CUL3–RBX1–KLHL22 proteins were sufficient to promote DEPDC5 ubiquitination in vitro (Extended Data Fig. 2c, d).

Several lysine residues were predicted by UbPred[16], or have previously been identified by mass spectrometry as possible ubiquitination sites of DEPDC5[17] (Extended Data Fig. 3a). K48-linked polyubiquitination and degradation of DEPDC5, and subsequent mTORC1 activation (indicated by S6K1 phosphorylation), were blocked if all five lysine residues were simultaneously mutated to arginine (5KR) (Extended Data Fig. 3b, c). However, none of the single mutations blocked DEPDC5 ubiquitination and degradation (Extended Data Fig. 3d, e). Therefore, CUL3–KLHL22 E3 ligase catalyses K48-linked ubiquitination on multiple sites of DEPDC5.

We next investigated how KLHL22 regulates DEPDC5 in response to amino acid availability. KLHL22 interacted specifically with DEPDC5 in an amino-acid-sensitive manner (Fig. 1h and Extended Data Fig. 4a–c). The direct interaction between DEPDC5 and KLHL22 was further demonstrated using recombinant proteins in an in vitro binding assay (Extended Data Fig. 4d). However, the DEPDC5(5KR) mutant was not able to interact with KLHL22 (Extended Data Fig. 4d), possibly owing to the aberrant folding of DEPDC5 caused by the mutations. Therefore, the lysine residues responsible for DEPDC5 ubiquitylation by KLHL22 warrant further investigation. Through truncation mapping tests, the DEP domain was identified as the degron of DEPDC5 (Extended Data Fig. 4e, f), which is responsible for KLHL22-mediated degradation (Extended Data Fig. 4g). Mutation of each serine, threonine, or tyrosine within the degron did not prevent its interaction with KLHL22 (Extended Data Fig. 4h), suggesting that it might not be a phospho-degron.

To understand how amino acids modulate KLHL22 activity, we monitored the localization of KLHL22 in response to amino acids. Notably, amino acids mediated nuclear–cytosolic shuttling of KLHL22 (Extended Data Fig. 5a, b). Several phosphorylation sites have been reported in KLHL22[11] (Extended Data Fig. 5c). We mutated each site to alanine, and found that S18 was required for the nuclear accumulation of KLHL22 in amino-acid-deprived conditions (Extended Data Fig. 5d). Through mass spectrometry analysis, we found that KLHL22 associated with 14-3-3 proteins during amino acid starvation (Extended Data Fig. 5e). The S18A mutation disrupted the interaction between

[1]State Key Laboratory of Membrane Biology, Institute of Molecular Medicine, Peking-Tsinghua Center for Life Sciences, Beijing Key Laboratory of Cardiometabolic Molecular Medicine, Peking University, Beijing, China. [2]Academy for Advanced Interdisciplinary Studies, Peking University, Beijing, China. [3]College of Biological Science and Technology, Beijing Forestry University, Beijing, China. [4]Key Laboratory of Carcinogenesis and Translational Research (Ministry of Education), Breast Center, Peking University Cancer Hospital & Institute, Beijing, China.
*e-mail: ying.liu@pku.edu.cn
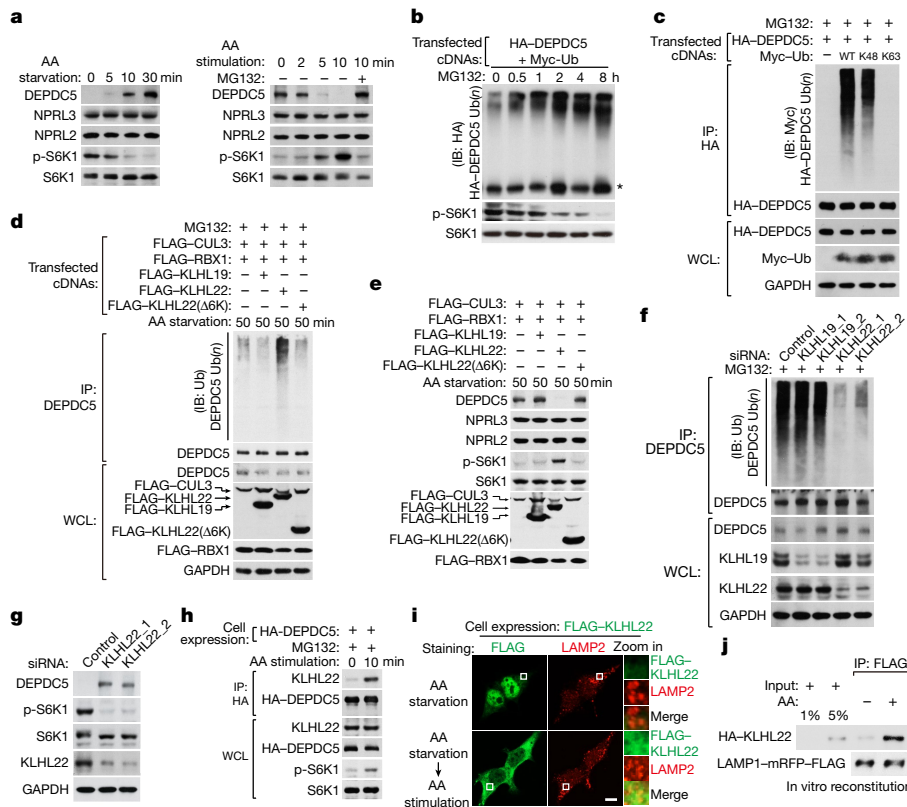
Fig. 1 | CUL3–KLHL22 mediates K48-linked polyubiquitination and degradation of DEPDC5. a, DEPDC5 is regulated in an amino-acid-sensitive manner. AA, amino acid. **b**, Accumulation of ubiquitinated DEPDC5 upon MG132 treatment. The asterisk represents HA–DEPDC5. IB, immunoblot; Ub(n), polyubiquitinated. **c**, DEPDC5 is modified by K48-linked polyubiquitination. IP, immunoprecipitation; WCL, whole-cell lysate. **d**, **e**, CUL3–KLHL22 promotes the ubiquitination (**d**) and degradation (**e**) of DEPDC5. **f**, **g**, Knockdown of KLHL22 suppresses the ubiquitination (**f**) and degradation (**g**) of DEPDC5. **h**, KLHL22 interacts with DEPDC5 in an amino-acid-dependent manner. **i**, KLHL22 partially locates on lysosomes under amino-acid-sufficient conditions. LAMP2, lysosome. Scale bar, 10 μm. **j**, Recombinant KLHL22 accumulates on purified lysosomes in response to amino acids. For gel source data, see Supplementary Fig. 1.

KLHL22 and 14-3-3, leading to the constitutive activation of mTORC1 (Extended Data Fig. 5f, g). Therefore, during amino acid starvation, KLHL22 was trapped by 14-3-3 proteins in the nucleus. Upon amino acid stimulation, KLHL22 was released and translocated to the cytosol. Once in the cytosol, KLHL22 localized at least in part to the lysosome (Fig. 1i), where GATOR1 resides[10,18]. Consistently, KLHL22 accumulated on purified lysosomes in the in vitro reconstitution system when amino acids were supplemented (Fig. 1j and Extended Data Fig. 5h, i).

Recruitment of mTORC1 to the surface of lysosomes is a key step for amino-acid-induced mTORC1 activation[5]. In KLHL22 knockout cells (sgKLHL22), mTORC1 could not accumulate on lysosomes upon amino acid stimulation (Fig. 2a and Extended Data Fig. 6a, b). In addition, in KLHL22 knockout cells, amino acid replenishment was not able to reduce the DEPDC5 level or activate mTORC1 (Fig. 2b). Conversely, ectopic expression of CUL3–KLHL22 induced S6K1 phosphorylation (Fig. 2c). Overexpression or depletion of KLHL22 did not perturb mTORC1 signalling in DEPDC5-deficient cells (Extended Data Fig. 6c, d), further suggesting that KLHL22 regulates the mTORC1 pathway through modulation of DEPDC5.

Expression of dominant-negative Rag GTPases (Rag[DN])[5,6] completely blocked KLHL22-mediated mTORC1 activation (Fig. 2c), indicating that KLHL22 acts upstream of Rag GTPases to mediate mTORC1 signalling. Consistently, KLHL22 displayed nuclear–cytosolic shuttling and activated mTORC1 in response to leucine but not glutamine, an amino acid that activates mTORC1 in a Rag-independent fashion[19] (Fig. 2d, e). mTORC1 negatively regulates catabolic pathways such as autophagy[20]. Deletion of KLHL22 activated autophagy, as determined by the increased LC3BII/I ratio (Fig. 2f and Extended Data Fig. 6e) and the induction of LC3B puncta (Fig. 2g and Extended Data Fig. 6f). KLHL22 deficiency also reduced cell size (Fig. 2h), a phenotypic

characteristic of mTORC1 inactivation[21]. Thus, KLHL22 is essential for the activation of mTORC1 and downstream events.

To investigate whether KLHL22 plays an evolutionarily conserved role in TORC1 signalling, we knocked out KLHL22 in mouse embryonic fibroblast (MEF) cells, and showed that mTORC1 failed to accumulate on lysosomes and phosphorylate S6K1 upon amino acid stimulation (Fig. 3a, b and Extended Data Fig. 7a). Multiple genes are predicted as potential *KLHL22* orthologues in *C. elegans* (Extended Data Fig. 7b). We screened these genes with the use of a reporter strain expressing GFP-tagged HLH-30, an orthologue of human transcription factor EB (TFEB) that translocalizes to the nucleus upon TORC1 inhibition[22,23]. Knockdown of *mel-26* or *tag-53*, but not any other gene, induced the nuclear accumulation of HLH-30 (Fig. 3c and Extended Data Fig. 7c). RNAi knockdown of *T08A11.1*, which encodes the orthologue of human DEPDC5, impaired HLH-30 nuclear localization in *mel-26*-deficient animals, but not in *tag-53*-deficient worms (Fig. 3d and Extended Data Fig. 7c). Downregulation of *T08A11.1* also restored the developmental delay of *mel-26*-deficient worms (Extended Data Fig. 7d). More importantly, expression of codon-optimized human KLHL22 suppressed the nuclear accumulation of HLH-30 in *mel-26* mutant animals (Fig. 3e), suggesting that MEL-26 functions as the *C. elegans* orthologue of KLHL22 to regulate T08A11.1 (*Ce*.DEPDC5).

Inhibition of TORC1 has been linked with lifespan extension in several species[24–27]. To determine the physiological significance of KLHL22, we compared the lifespans of wild-type worms with those of *mel-26* mutants. Deletion of *mel-26* significantly extended worm lifespan (Fig. 3f). The prolonged lifespan of *mel-26* mutants was suppressed by RNAi knockdown of *T08A11.1* (Fig. 3g).

The mTORC1 pathway is frequently deregulated in many cancer types[8,9]. Deletions in GATOR1 subunits NPRL2 and DEPDC5 have
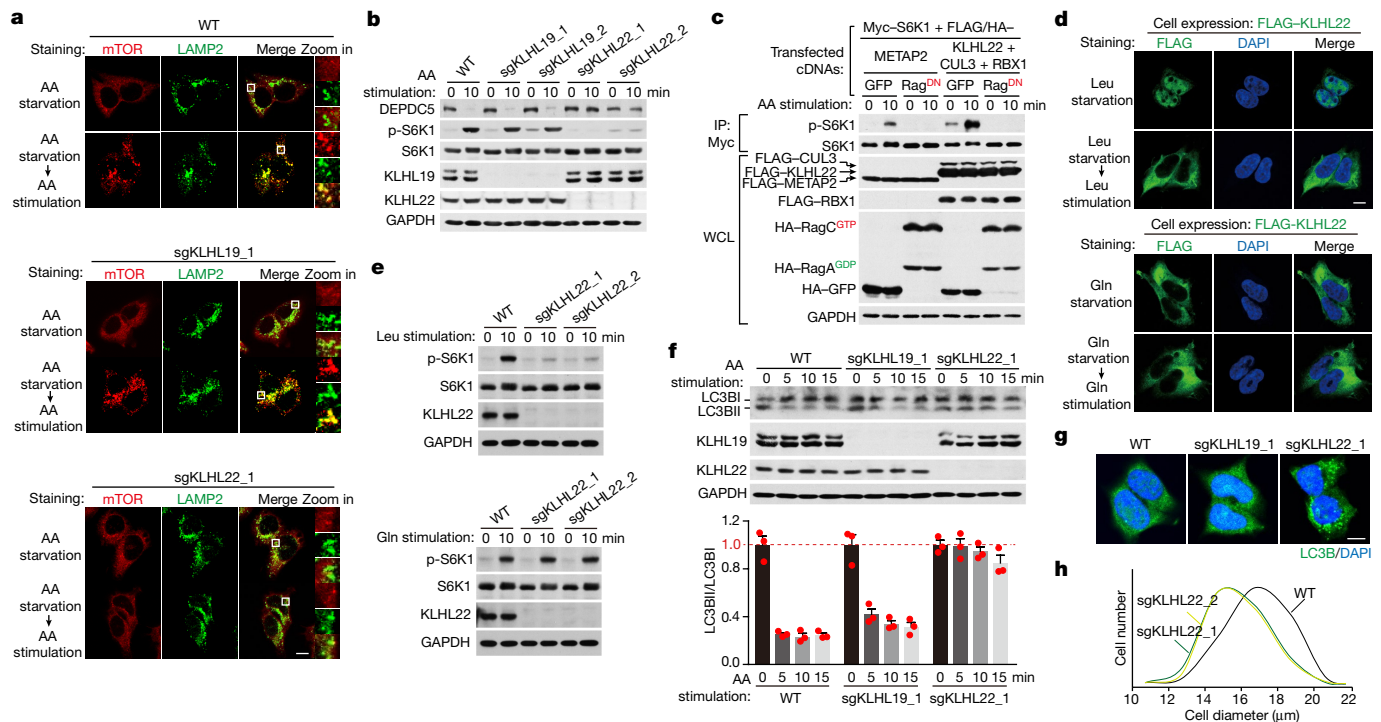
Fig. 2 | KLHL22 is required for mTORC1 activation, autophagy and cell growth. a, KLHL22 depletion prevents amino-acid-stimulated lysosomal accumulation of mTORC1. Scale bar, 10 μm. **b**, Depletion of KLHL22 suppresses amino-acid-dependent degradation of DEPDC5 and phosphorylation of S6K1. WT, wild-type. **c**, KLHL22 plays a role upstream of Rag GTPases. Rag^{DN}: RagA^{GDP}–RagC^{GTP}, dominant-negative form of Rag GTPases. **d**, FLAG–KLHL22 translocates to the cytosol upon stimulation with leucine but not glutamine. DAPI, nuclei. Scale bar, 10 μm. **e**, Deprivation of KLHL22 prevents leucine-induced but not glutamine-induced S6K1 phosphorylation. **f**, KLHL22 is required for amino-acid-induced suppression of autophagy. $n = 3$ biologically independent experiments. **g**, Depletion of KLHL22 induces formation of LC3B puncta. DAPI, nuclei. Scale bar, 10 μm. **h**, Depletion of KLHL22 reduces cell size. For gel source data, see Supplementary Fig. 1.

been reported in lung and breast cancers, and two cases of glioblastoma[28–30]. Overexpression of DEPDC5 reduced cell size (Extended Data Fig. 8a), whereas co-expression of KLHL22 restored it (Extended Data Fig. 8b). Furthermore, a stable HEK293T cell line with a high level

of KLHL22 showed greatly altered growth morphology and increased anchorage-independent growth (Fig. 4a, b and Extended Data Fig. 8c). High-level expression of KLHL22 conferred increased sensitivity to rapamycin, an mTORC1 inhibitor (Fig. 4b).
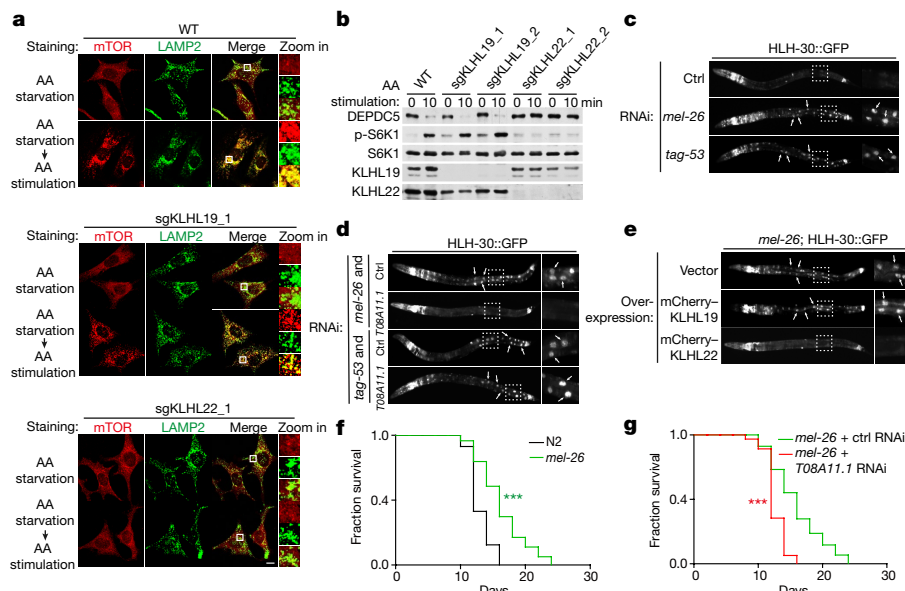
Fig. 3 | KLHL22 plays an evolutionarily conserved role in the regulation of DEPDC5. a, KLHL22 is required for amino-acid-induced lysosomal localization of mTOR in MEF cells. Scale bar, 10 μm. **b**, Deficiency of KLHL22 suppresses amino-acid-induced degradation of DEPDC5 and phosphorylation of S6K1 in MEF cells. For gel source data, see Supplementary Fig. 1. **c**, RNA interference (RNAi) targeting *mel-26* or *tag-53* induces nuclear accumulation of HLH-30::GFP in *C. elegans* (arrows). Dashed boxes are expanded on right. **d**, RNAi targeting *T08A11.1* suppresses nuclear accumulation of HLH-30 in *mel-26*-deficient, but not *tag-53*-deficient worms. **e**, Human KLHL22 prevents the nuclear accumulation of HLH-30 in *mel-26*-deficient worms. **f**, **g**, *mel-26* mutant worms have prolonged lifespan (**f**) and RNAi of *T08A11.1* suppresses lifespan extension in *mel-26* mutant worms (**g**). $n = 2$ biologically independent experiments. ***P < 0.001; log rank test of one replicate is shown.
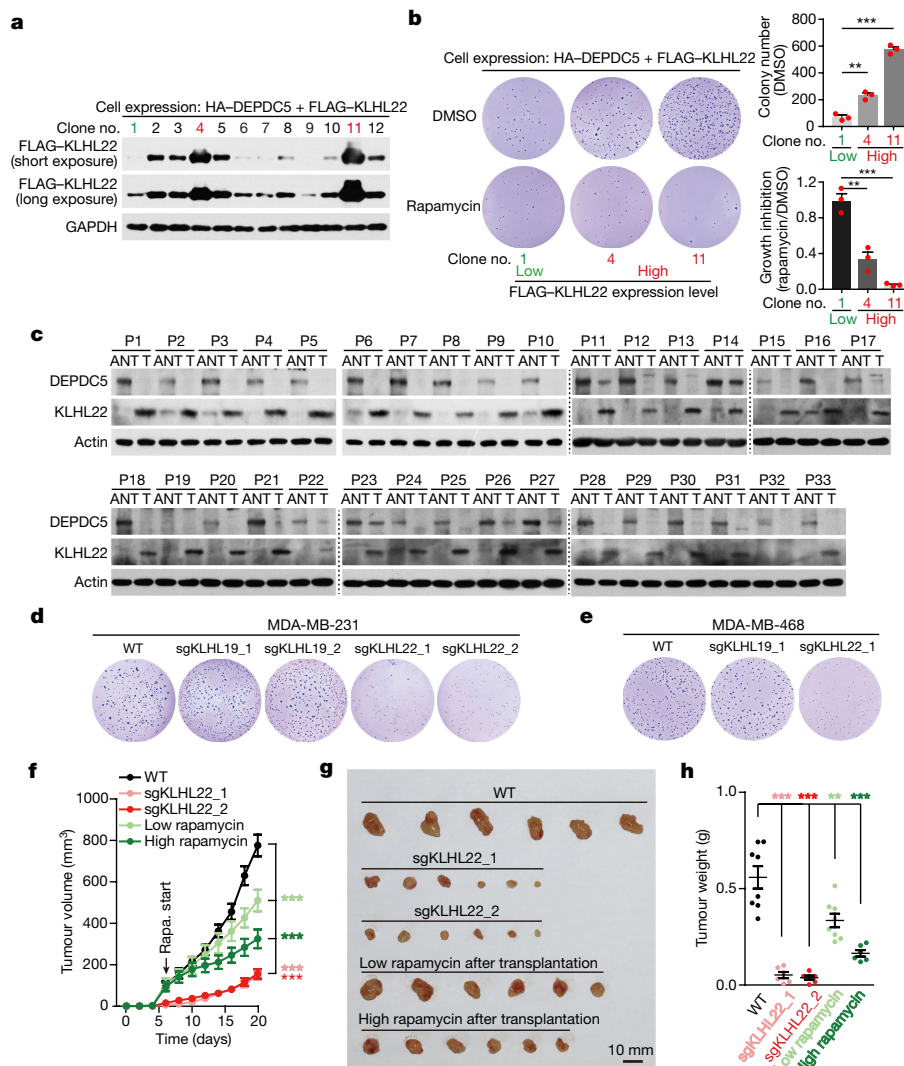
Fig. 4 | KLHL22 acts as a potential oncogene in breast cancer. a, Protein levels of FLAG–KLHL22 in cells stably expressing HA–DEPDC5 and FLAG–KLHL22. Green or red denotes low or high protein level of KLHL22. **b**, High levels of KLHL22 promote anchorage-independent growth and confer increased rapamycin sensitivity. $n = 3$ biological replicates. **P < 0.01; ***P < 0.001, two-sided Student's t-test. **c**, Upregulation of KLHL22 and downregulation of DEPDC5 are detected in tumours of breast cancer patients. T, tumour; ANT, adjacent normal tissues; P1, pair 1. **d**, **e**, Depletion of KLHL22 inhibits anchorage-independent growth of MDA-MB-231 (**d**) and MDA-MB-468 (**e**) human breast cancer cells. **f–h**, Deletion of KLHL22 or treatment with rapamycin suppresses tumour growth of MDA-MB-231 cells. Tumour volume, mean ± s.e.m. ($n = 9$ mice for sgKLHL22_2, $n = 10$ mice for remaining groups), ***P < 0.001, two-sided ANOVA (**f**); tumour images (**g**); and tumour weights 20 d after transplantation, mean ± s.e.m. ($n = 8$ mice for WT and WT injected with low dose of rapamycin, $n = 6$ mice for remaining groups), ***P < 0.001, two-sided Student's t-test (**h**). For gel source data, see Supplementary Fig. 1.

The 'Oncomine' database revealed several cancer types with elevated KLHL22 transcript levels (Extended Data Fig. 8d). Protein levels of KLHL22 were elevated in multiple breast cancer cell lines, such as MDA-MB-231, MDA-MB-468 and BT549, compared with the corresponding control cell line MCF10A (Extended Data Fig. 8e). More strikingly, the level of KLHL22 protein was markedly increased in breast tumours of patients, in comparison with that of the adjacent normal tissues (Fig. 4c). The elevation of KLHL22 correlated strongly with a reduction in DEPDC5 protein level in each tumour sample (Fig. 4c). KLHL22 mRNA level was also elevated in tumour samples (Extended Data Fig. 8f), suggesting that KLHL22 might be regulated at the transcriptional level in breast cancer.

Breast cancer cells (for example, MDA-MB-231) displayed similar regulation of DEPDC5 in response to amino acids (Extended Data Fig. 8g–i). Thus, to test whether KLHL22 promotes tumour growth, we knocked out KLHL22 in MDA-MB-231 and MDA-MB-468, two breast cancer cell lines with elevated KLHL22 levels (Extended Data Figs 9a–c). Depletion of KLHL22 suppressed amino acid-triggered degradation of DEPDC5 and phosphorylation of S6K1, and inhibited anchorage-independent growth of both cell lines (Fig. 4d, e and Extended Data Fig. 9d, e). Finally, we subcutaneously transplanted wild-type MDA-MB-231 and MDA-MB-468 cells, or KLHL22 knockout cells, into immunodeficient nude mice. Depletion of KLHL22 significantly prevented tumour growth (Fig. 4f–h, Extended Data Fig. 9f–h). Moreover, treatment with rapamycin suppressed tumour growth (Fig. 4f–h, Extended Data Fig. 9i–k). Collectively, these data demonstrate that KLHL22 functions as a potential oncogene to active mTORC1 signalling and promote tumour growth in breast cancer.

In response to amino acids, the inhibitory function of GATOR1 must be released in order to activate mTORC1. The identification of CUL3–KLHL22 E3 ubiquitin ligase provides a novel mechanism for amino-acid-induced GATOR1 inactivation. KLHL22 promotes ageing in *C. elegans*, and tumour growth in mice, adding to the physiological significance of this regulation (Extended Data Fig. 10). Strikingly, tumour samples from breast cancer patients all have elevated KLHL22 protein levels, which is correlated with the reduction in DEPDC5

levels. Small molecules that inhibit KLHL22 activity on DEPDC5 are candidates for development as drugs for the treatment of breast cancer and age-related diseases.

Online content

1. Dibble, C. C. & Manning, B. D. Signal integration by mTORC1 coordinates nutrient input with biosynthetic output. *Nat. Cell Biol.* **15**, 555–564 (2013).
2. Laplante, M. & Sabatini, D. M. mTOR signaling in growth control and disease. *Cell* **149**, 274–293 (2012).
3. Yuan, H. X., Xiong, Y. & Guan, K. L. Nutrient sensing, metabolism, and cell growth control. *Mol. Cell* **49**, 379–387 (2013).
4. Zoncu, R., Efeyan, A. & Sabatini, D. M. mTOR: from growth signal integration to cancer, diabetes and ageing. *Nat. Rev. Mol. Cell Biol.* **12**, 21–35 (2011).
5. Kim, E., Goraksha-Hicks, P., Li, L., Neufeld, T. P. & Guan, K. L. Regulation of TORC1 by Rag GTPases in nutrient response. *Nat. Cell Biol.* **10**, 935–945 (2008).
6. Sancak, Y. et al. The Rag GTPases bind raptor and mediate amino acid signaling to mTORC1. *Science* **320**, 1496–1501 (2008).
7. Bar-Peled, L. et al. A tumor suppressor complex with GAP activity for the Rag GTPases that signal amino acid sufficiency to mTORC1. *Science* **340**, 1100–1106 (2013).
8. Sabatini, D. M. mTOR and cancer: insights into a complex relationship. *Nat. Rev. Cancer* **6**, 729–734 (2006).
9. Guertin, D. A. & Sabatini, D. M. Defining the role of mTOR in cancer. *Cancer Cell* **12**, 9–22 (2007).
10. Wolfson, R. L. et al. KICSTOR recruits GATOR1 to the lysosome and is necessary for nutrients to regulate mTORC1. *Nature* **543**, 438–442 (2017).
11. Mertins, P. et al. Proteogenomics connects somatic mutations to signalling in breast cancer. *Nature* **534**, 55–62 (2016).
12. Petroski, M. D. & Deshaies, R. J. Function and regulation of cullin-RING ubiquitin ligases. *Nat. Rev. Mol. Cell Biol.* **6**, 9–20 (2005).
13. Dhanoa, B. S., Cogliati, T., Satish, A. G., Bruford, E. A. & Friedman, J. S. Update on the Kelch-like (KLHL) gene family. *Hum. Genomics* **7**, 13 (2013).
14. Pintard, L., Willems, A. & Peter, M. Cullin-based ubiquitin ligases: Cul3-BTB complexes join the family. *EMBO J.* **23**, 1681–1687 (2004).
15. Beck, J. et al. Ubiquitylation-dependent localization of PLK1 in mitosis. *Nat. Cell Biol.* **15**, 430–439 (2013).
16. Radivojac, P. et al. Identification, analysis, and prediction of protein ubiquitination sites. *Proteins* **78**, 365–380 (2010).
17. Wagner, S. A. et al. A proteome-wide, quantitative survey of in vivo ubiquitylation sites reveals widespread regulatory roles. *Mol. Cell. Proteomics* **10**, M111–013284 (2011).
18. Peng, M., Yin, N. & Li, M. O. SZT2 dictates GATOR control of mTORC1 signalling. *Nature* **543**, 433–437 (2017).
19. Jewell, J. L. et al. Metabolism. Differential regulation of mTORC1 by leucine and glutamine. *Science* **347**, 194–198 (2015).
20. Hosokawa, N. et al. Nutrient-dependent mTORC1 association with the ULK1-Atg13-FIP200 complex required for autophagy. *Mol. Biol. Cell* **20**, 1981–1991 (2009).
21. Fingar, D. C., Salama, S., Tsou, C., Harlow, E. & Blenis, J. Mammalian cell size is controlled by mTOR and its downstream targets S6K1 and 4EBP1/eIF4E. *Genes Dev.* **16**, 1472–1487 (2002).
22. Lapierre, L. R. et al. The TFEB orthologue HLH-30 regulates autophagy and modulates longevity in *Caenorhabditis elegans*. *Nat. Commun.* **4**, 2267 (2013).
23. Settembre, C. et al. A lysosome-to-nucleus signalling mechanism senses and regulates the lysosome via mTOR and TFEB. *EMBO J.* **31**, 1095–1108 (2012).
24. Kaeberlein, M. et al. Regulation of yeast replicative life span by TOR and Sch9 in response to nutrients. *Science* **310**, 1193–1196 (2005).
25. Vellai, T. et al. Genetics: influence of TOR kinase on lifespan in *C. elegans*. *Nature* **426**, 620 (2003).
26. Kapahi, P. et al. Regulation of lifespan in *Drosophila* by modulation of genes in the TOR signaling pathway. *Curr. Biol.* **14**, 885–890 (2004).
27. Harrison, D. E. et al. Rapamycin fed late in life extends lifespan in genetically heterogeneous mice. *Nature* **460**, 392–395 (2009).
28. Lerman, M. I. & Minna, J. D. The 630-kb lung cancer homozygous deletion region on human chromosome 3p21.3: identification and evaluation of the resident candidate tumor suppressor genes. The International Lung Cancer Chromosome 3p21.3 Tumor Suppressor Gene Consortium. *Cancer Res.* **60**, 6116–6133 (2000).
29. Li, J. et al. Functional characterization of the candidate tumor suppressor gene NPRL2/G21 located in 3p21.3C. *Cancer Res.* **64**, 6438–6443 (2004).
30. Seng, T. J. et al. Complex chromosome 22 rearrangements in astrocytic tumors identified using microsatellite and chromosome 22 tile path array analysis. *Genes Chromosom. Cancer* **43**, 181–193 (2005).

Author contributions J.C., assisted by Y.O., performed most of the experiments and analysed the data. Y.Y. generated the *mel-26*; HLH-30::GFP strain. W.L. generated DEPDC5 and KLHL22 point mutation constructs. Y.Xu. and Y.Xi. provided breast cancer samples. J.C. and Y.L. wrote the manuscript.

METHODS

Antibodies. Anti-HA (Santa Cruz 7392), anti-FLAG (Sigma F7425), anti-LAMP2 (IF in HEK293T, Abcam 25631), anti-LAMP2 (IF in MEF, Abcam 13524), anti-mTOR (CST 2983), anti-LC3B (Sigma L7543), anti-Myc (ImmunoWay YM3203), anti-Ub (Santa Cruz 8017), anti-KLHL22 (Proteintech 16214-1-AP), anti-KLHL19 (Proteintech10503-2-AP), anti-NPRL2 (Sigma SAB1305758), anti-NPRL3 (Sigma HPA011741), anti-DEPDC5 (Sigma SAB1302644), anti-p-S6K1 (CST 9205), anti-S6K1 (CST 9202), anti-PDI (Santa Cruz 20132), anti-Prohibitin (Santa Cruz 28259), anti-EEA1 (CST 3288), anti-GAPDH (Abcam 128915), anti-Lamin B1 (Bioworld MB2029), anti-Histone H3 (CST 3638), anti-Actin (Sigma A5441), and anti-14-3-3 (Santa Cruz 23957) were used.

Cell lines and cell culture. MCF10A, MCF7, SKBR3, BT549, PWR1E, 22RV1, LNCAP and HSF cells were provided by G. Ouyang (Xiamen University); A375 and MV3 cells were provided by Q. Wu (Xiamen University); MDA-MD-231, MDA-MB-468, PC3 and MEF cells were gifts from S.-C. Lin (Xiamen University). HEK293T cells were purchased from ATCC. None of the cell lines in this study appears in the misidentified cell line list kept by the ICLAC. Cell lines served in this study were not authenticated immediately before use in our laboratory. All cell lines were validated to be free of mycoplasma contamination.

All cell lines were maintained at 37 °C and 5% CO_2, with the exception of MDA-MB-231 and MDA-MB-468 cells, which were cultured without CO_2. MCF10A cells were maintained in MEBM medium (Lonza) supplemented with its additives (without using GA-1000) and 100 ng/ml cholera toxin (Sigma). MCF7 cells were maintained in MEM medium (Gibco) supplemented with 10% inactivated fetal bovine serum (FBS), penicillin and streptomycin (P/S). PC3, 22RV1, LNCAP and BT549 cells were kept in RPMI1640 medium (Gibco) supplemented with 10% FBS and penicillin/streptomycin (P/S). PWR1E, A375, HSF, MV3, MEF and HEK293T cells and their derivatives were maintained in DMEM high glucose medium (Hyclone) supplemented with 10% FBS and P/S. SKBR3 cells were cultured in McCoy's 5a medium (Gibco) supplemented with 10% FBS and P/S. MDA-MB-231 and MDA-MB-468 cells and their derivatives were kept in L15 medium (Gibco) supplemented with 10% FBS and P/S. Except where indicated, data were generated using HEK293T cells.

For amino acid (AA), leucine or glutamine starvation, cells were incubated in handmade DMEM base medium lacking AAs, leucine or glutamine for the indicated times. For AA, leucine or glutamine stimulation, cells were starved for 50 min and then stimulated by directly adding AAs, leucine or glutamine high concentration stock solution for the indicated times. For starvation and re-stimulation experiments in Fig. 1a and Extended Data Fig. 1f, 5a, dialysed FBS (Gibco, 26400044) was supplemented. For starvation and stimulation experiments in the remaining figures, insulin (Sigma, I9278) was supplemented at 200 ng/ml. High concentration AA solution is a combination of commercial 50 × glutamine-free AA mixture (Gibco, 11130051) and 50 × glutamine (Gibco, 25030081). High concentration leucine and glutamine solutions were handmade.

For drug treatments, MG132 dissolved in DMSO (Santa Cruz 201270) was pre-diluted with medium to 10 μg/ml. Medium containing MG132 was then used to replace the original medium and cells were cultured in the presence of MG132 for 1 h. When supplemented along with amino acids, MG132 was continuously present during starvation, or starvation and re-stimulation periods. Chloroquine (CQ) (Sigma C6628) or cycloheximide (CHX) (Sigma, C7698) dissolved in water was added directly into the culturing medium at a final concentration of 50 μM or 50 μg/ml, respectively.

Nematode strains and culture conditions. *C. elegans* strains (N2; EU1007: *mel-26*; MAH240: HLH-30::GFP) were obtained from the *Caenorhabditis* Genetics Center (CGC). N2 and HLH-30::GFP strains were cultured at 20 °C. *mel-26* mutants were maintained at 15 °C. For lifespan analysis, temperature-sensitive *mel-26* mutants and the corresponding controls were cultured at 25 °C in the presence of fluorodeoxyuridine (FUDR). For RNAi-mediated gene knockdowns, HLH-30::GFP reporter worms were cultured at 20 °C.

Generation of KLHL19 or KLHL22 knock-out cells. CRISPR guide sequences targeting the second exon of *KLHL19* or *KLHL22* were designed by http://crispr.mit.edu and cloned into pBC2 CRISPR vectors that were provided by Y. Wang (Peking University). Sequences were as follows: sgKLHL19_1_human: 5′ TTGGCATCATGAACGAGCTG 3′; sgKLHL19_2_human: 5′ GGATGCACC GGCCGCCCAGT 3′; sgKLHL22_1_human: 5′ CACTGCGTGAACAACACCTA 3′; sgKLHL22_2_human: 5′ GGACAGCGGAATCCTCTTCG 3′; sgDEP DC5_1_human: 5′ GTGTTCCCTCACATCAAGCT 3′; sgDEPDC5_2_human: 5′ AGGATCAGTATATTGGCCGT 3′; sgKLHL19_1_mouse: 5′ TCGCAGGACGG TAACCGAAC 3′; sgKLHL19_2_mouse: 5′ GGGACGCAGTGATGTATGCC 3′; sgKLHL22_1_mouse: 5′ ATCGGATTCTGCTAGCTGCA 3′; sgKLHL22_2_ mouse: 5′ GATCCTCTTTGACGTTGTCC 3′·HEK293T, MEF, MDA-MB-231 or MDA-MB-468 cells were cultured in 6-well plates and transfected with the corresponding CRISPR vector. Cells were trypsinized 48 h later and 250 μg/ml hygromycin was added into the culturing medium. Hygromycin-resistant cells were then sorted into 96-well plates and validated by genotyping.

Generation of stable cell lines. HEK293T stable cell lines were generated using a lentiviral system. The following lentiviral expression constructs were used: pBOBE-HA-DEPDC5, pBOBE-Myc-Ub, pBOBE-Myc-K48Ub, pBOBE-FLAG-KLHL22 and pLJM1-LAMP1-mRFP-FLAG$^{×2}$. The pBOBE vector was a gift from S.-C. Lin (Xiamen University). HEK293T cells in 6-well plates were transfected with the plasmids indicated above, together with pMDLg/pRRE, pRSV-Rev and pCI-VSVG. Medium was changed 8 h after transfection. Cells were then cultured for an additional 24 h to allow virus production (virus packaging). HEK293T cells were cultured in virus-containing medium supplemented with 8 μg/ml polybrene for 24 h (virus infection). G418 was added to the culturing medium for selection.

Immunoprecipitation. Cells were lysed on ice for 40 min using TX-100 lysis buffer (20 mM Tris-HCl, 150 mM NaCl, 1 mM Na_2EDTA, 1 mM EGTA, 2.5 mM sodium pyrophosphate, 1 mM β-glycerophosphate, 1% Triton X-100, pH 7.4) supplemented with EDTA-free protease inhibitors (Roche). Cell lysates were then centrifuged at 12,000 r.p.m. for 10 min at 4 °C. For anti-FLAG and anti-HA immunoprecipitation, supernatants of cell lysates were supplemented with washed FLAG or HA affinity gels (Sigma/Pierce) and rotated at 4 °C for 2 h. Immunoprecipitates were then washed three times with TX-100 lysis buffer. Whole cell lysates and immunoprecipitates were analysed by immunoblotting.

For transfection-based experiments, HEK293T cells were plated in 6-cm dishes and transfected with pcDNA3.3-based expression vectors using polyethylenimine (PEI) transfection reagent. 48 h after transfection, cells were subjected to treatments and then processed as described above.

Ubiquitination assays. HEK293T cells with or without the expression of exogenous proteins were lysed on ice for 10 min with RIPA lysis buffer (20 mM Tris-HCl, 150 mM NaCl, 1 mM Na_2EDTA, 1 mM EGTA, 1% NP-40, 1% sodium deoxycholate, 2.5 mM sodium pyrophosphate, 1 mM β-glycerophosphate) containing 1% SDS supplemented with EDTA-free protease inhibitors (Roche). Cell lysates were briefly sonicated, boiled at 100 °C for 10 min, and then centrifuged at 12,000 r.p.m. for 10 min at 4 °C. Supernatants were then diluted 1:3 with RIPA lysis buffer to reduce the concentration of SDS. For ubiquitination assay of HA-tagged DEPDC5, pre-washed HA affinity gels were incubated with diluted lysates for 2 h at 4 °C. For ubiquitination assay of endogenous DEPDC5, anti-DEPDC5 antibodies were added into diluted lysates for overnight binding. Protein G beads were then incubated with lysates at 4 °C for 1 h to enrich anti-DEPDC5 antibodies. Immunoprecipitates were washed three times with RIPA lysis buffer containing 0.1% SDS and analysed by immunoblotting.

For knockdown experiments, siRNAs were transfected using the RNAiMAX transfection reagent (Thermo). 48 h after transfection, cells were subjected to ubiquitination assays. Sequences of siRNAs were as follows: siKLHL19_1: 5′ GGGAGTACATCTACATGCATT 3′; siKLHL19_2: 5′ GAGTGTTACGACCCAGATA 3′; siKLHL22_1: 5′ CAGGCTACGTGCACATTTA 3′; siKLHL22_2: 5′ GCTCAACAACTTCGTATAC 3′.

For in vitro ubiquitination assays, 2.5 μl GST-CUL3/RBX1 (BPS Bioscience) mixed with 2 μg FLAG–KLHL19 or FLAG–KLHL22 purified from HEK293T cells was used. The E3 ligase complex was mixed with 2 μg HA–DEPDC5 purified from HEK293T cells, 15 μg wild-type ubiquitin or K48R ubiquitin, 550 ng E1 (UBE1), 850 ng E2 (UBE2D2), 12.5 mM Mg-ATP and 1 × ubiquitin reaction buffer, and incubated at 37 °C for 1 h. The above reagents except for the annotated ones were purchased from Boston Biochem. Reactions were terminated by boiling at 100 °C with SDS sample buffer for 10 min and analysed by immunoblotting.

RNA extraction and quantification. Cells or worms were lysed with TRIzol Reagent. Total RNA was isolated by chloroform extraction and isopropanol precipitation. One migrogram total RNA was used for reverse transcription using a cDNA synthesis kit (TransGen Biotech). cDNAs of each gene were quantified by PCR or real-time PCR (qPCR). For PCR, amplifications of cDNAs were resolved by agarose gel. For qPCR, quantifications of transcripts were normalized to GAPDH. The following primers were used: *DEPDC5*: 5′ACCAGACTGTGACTCAAGTG and 5′ATAGGCACATGTGCTGACC; *GAPDH*: 5′ACCACAGTCCATGCCATCAC and 5′TCCACCACCC TGTTGCTGTA; *ACTβ*: 5′ATCTGGCACCACACCTTCTAC and 5′GGATA GCAACGTACATGGCTG; *KLHL19*: 5′GTGCTGTCATGTACCAGATC and 5′GGTTGAAGAACTCCTCTTGC; *KLHL22*: 5′GAGAGTGGAAGC ACTTCACTG and 5′GCGTAGATGTACCTGCCTACA; *mel-26*: 5′CGAGC TGTTACGTACATCCTG and 5′AGTCCAGATGGAGGTGGTAC; *tag-53*: 5′CGCTTTGATCACACAGTTGTC and 5′TCACATGAGCTGAGTGACCTG; *T08A11.1*: 5′TCTGTGCTCACGGTGGTATG and 5′CGAATTGAACCTGT GGAAGC; *rpl-32*: 5′AGGGAATTGATAACCGTGTCCG and 5′TAGGA CTGCATGAGGAGCATGT.

Nuclear/cytosolic fractionation. After amino acid treatment, cells in 6-well plates were lysed on ice for 10 min with 200 μl per well NP-40 lysis buffer (10 mM Tris-HCl, 150 mM NaCl, 0.05% NP-40) supplemented with EDTA-free protease inhibitors (Roche). Samples were centrifuged at 5,000 r.p.m. for 5 min at 4 °C to isolate the pellets (nuclei) and supernatants (cytosol). Nuclear and cytosolic fractions were boiled with SDS sample buffer and then analysed by immunoblotting.

Purification of recombinant proteins. Recombinant human HA–DEPDC5, FLAG–KLHL22, FLAG–KLHL19 and HA–KLHL22 were immunopurified from HEK293T cells. For purification of each protein, 10×15-cm dishes of HEK293T cells transfected with corresponding expression vectors were lysed on ice for 40 min using TX-100 lysis buffer supplemented with EDTA-free protease inhibitors (Roche). Cell lysates were then centrifuged at 12,000 r.p.m. for 10 min at 4 °C. Supernatants were mixed with 300 μl HA or FLAG affinity gels and rotated at 4 °C for 2 h. Immunoprecipitates were washed three times with TX-100 lysis buffer and three times with PBS, and eluted in 500 μl PBS containing 100 μg/ml HA or FLAG peptides. Purified proteins were analysed by Commassie G250 staining and immunoblotting. For storage, purified proteins supplemented with 20% (v/v) glycerol were kept at −20 °C.

Silver staining and mass spectrometry. To identify interaction proteins of DEPDC5 or KLHL22, 5×15-cm dishes of HEK293T cells stably expressing HA–DEPDC5 or FLAG–KLHL22 were lysed with TX-100 lysis buffer containing EDTA-free protease inhibitors (Roche). Cell lysates were centrifuged at 12,000 r.p.m. for 10 min at 4 °C. HA or FLAG affinity gels were added to supernatants for immunoprecipitation. Immunoprecipitates were denatured by boiling in SDS sample buffer and resolved by SDS–PAGE. Silver staining was carried out according to the manufacturer's instructions (Sigma, PROTSIL2). For interaction partners of HA–DEPDC5, bands of interest were cut from the gel and analysed by mass spectrometry; for FLAG–KLHL22, the whole lane was analysed.

Immunostaining. HEK293T cells were cultured on polylysine-coated glass coverslips (Corning) in 12-well plates (70,000 cells per well). After amino acid treatment, cells on coverslips were washed once with PBS, fixed with 4% paraformaldehyde in PBS, washed again with PBS and permeabilized with 0.1% Triton X-100 in PBS. Cells were then washed, and blocked in PBS containing 5% BSA for 30 min at room temperature. The coverslips were then incubated in PBS containing primary antibodies (1:200 dilutions) at 4 °C overnight. Cell were then rinsed, and incubated with secondary antibodies in PBS (1:200 dilutions) for 2 h at room temperature. After washing, coverslips were mounted on slides using a mounting buffer containing DAPI (Thermo) and imaged on Zeiss Fluorescence Microscopes (Imager M2 for Fig. 3c–e; LSM 710 confocal microscopy for other Figures).

In vitro reconstitution assay. For immunopurification of lysosomes, HEK293T cells stably expressing LAMP1–mRFP–FLAG$^{\times 2}$ were used. For each sample, cells in one 10-cm dish were pelleted through centrifugation at 1,000 r.p.m. for 3 min at room temperature. Cell pellets were washed once with fractionation buffer (50 mM KCl, 90 mM K-gluconate, 1 mM EGTA, 5 mM MgCl$_2$, 50 mM sucrose, 5 mM glucose, 20 mM HEPES, pH 7.4; 2.5 mM ATP and protease inhibitors were added immediately before use), resuspended in 0.8 ml fractionation buffer, and then mechanically broken by spraying six times through a 23 G needle attached to a 1-ml syringe. Cell fractions were spun down at 2,000*g* for 10 min at 4 °C to pellet the nuclei, yielding a post-nuclei supernatant (PNS). The PNS was adjusted to 2 ml, supplemented with 50 μl anti-FLAG affinity gels and rotated at 4 °C for 2 h to enrich lysosomes.

Immunopurified lysosomes were washed and resuspended in 300 μl fractionation buffer supplemented with 250 μM GTP and 100 μM GDP, in the presence or absence of $1 \times$ amino acids. Lysosomes were then rotated at 650 r.p.m. on a thermomixer for 15 min at 37 °C (activation step). The reaction system was subsequently supplemented with 20 μl purified HA–KLHL22 and rotated for additional 25 min (binding step). Immunoprecipitates were washed, denatured and then analysed by immunoblotting.

In vitro binding assay. HEK293T cells in 10-cm dishes were transfected with vectors expressing HA–DEPDC5, HA–DEPDC5-5KR or HA–DEPDC7. 48 h after transfection, cells were lysed in 2 ml ice-cold TX-100 lysis buffer containing EDTA-free protease inhibitors (Roche). Cell lysates were centrifuged at 12,000 r.p.m. for 10 min at 4 °C. Supernatants were saved, supplemented with 30 μl anti-HA affinity beads, and rotated at 4 °C for 2 h. Immobilized HA–DEPDC5, HA–DEPDC5-5KR or HA–DEPDC7 was washed once in TX-100 lysis buffer, followed by three washes in TX-100 lysis buffer supplemented with 500 mM NaCl. TX-100 lysis buffer was then replaced with 88 μl binding buffer (40 mM HEPES, 2 mM EGTA, 2.5 mM MgCl$_2$, 0.3% CHAPS, pH 7.4). For in vitro binding assay, 88 μl immobilized HA–DEPDC5, HA–DEPDC5-5KR or HA–DEPDC7 was incubated with 12 μl immunopurified FLAG–KLHL22 and supplemented with 1% BSA and 2 mM DTT at 4 °C for 1 h. Samples were washed three times in binding buffer and subjected to immunoblotting.

Determination of cell size. Cells at the confluence of $\sim 4 \times 10^6$ per ml were subjected to cell diameter determination using an easy cell analyser (CountStar).

HLH-30::GFP nuclear translocation assay. HLH-30::GFP reporter strain was crossed with *mel-26* mutants to generate *mel-26*; HLH-30::GFP. HLH-30::GFP or *mel-26*; HLH-30::GFP reporter strains subjected to the indicated treatments were photographed using a Zeiss Imager M2 microscope. Representative images are shown.

RNAi in *C. elegans*. RNAi clones from the Ahringer Library were grown in LB containing 50 μg/ml carbenicillin at 37 °C overnight and then seeded onto worm plates with IPTG. Dried plates were kept at room temperature overnight to allow IPTG induction of dsRNA expression. Worms were then seeded onto RNAi plates. Knockdown efficiencies were measured using qPCR.

Lifespan analysis. To compare the lifespan of *mel-26* mutants with that of N2 worms, about 100 L4 stage (day 0) N2 or *mel-26* mutant worms were transferred to plates containing *E. coli* OP50 and FUDR to prevent reproduction, and cultured at 25 °C. For lifespan analysis of *mel-26* mutants with *T08A11.1* knockdown, about 100 L4 stage *mel-26* worms were transferred to plates containing bacteria HT115 expressing dsRNAs, and cultured at 25 °C. Worms were transferred to new plates and counted every other day. FUDR was omitted after day 12. Animals that did not move when gently prodded were scored as dead. Animals that crawled off the plate or died owing to vulva bursting were not included. Sample size was determined by reference to the literature. Worms were chosen in an unbiased fashion for experimental analysis to ensure randomization. The investigators who collected the data were blinded to genotype and treatment.

Anchorage-independent growth assays. For the bottom-layer agarose medium, a 1:1 mixture of 1% low melting point agarose (Sigma) and pre-warmed $2 \times$ culture medium (prepared from powdered DMEM or L15 medium, Gibco) was added to 6-well plates (1.5 ml per well) and solidified at 20 °C for 30 min. The 1:1 mixed 0.6% low melting point agarose and cells in $1 \times$ culture medium with or without 100 nM rapamycin were poured onto the solidified bottom medium and allowed to solidify at 20 °C for 30 min, forming the top-layer agarose medium. Concentrations of HEK293T cells and MDA-MB-231/468 cells in $1 \times$ medium were 6,500 cells per ml and 2,500 cells per ml. One-hundred microlitres per well of $1 \times$ culture medium was added twice weekly onto the top medium to prevent drying. Cells were cultured at 37 °C with 5% CO_2 for around two weeks for adequate colony formation. Colonies were stained with 0.005% crystal violet in 5% methanol and quantified using ImageJ.

Tumour transplantations. Trypsinized MDA-MB-231 or MDA-MB-468 cells were washed twice with PBS and concentrated to 10^6 per 100 μl in PBS. Cell suspensions were then mixed with equal volumes of Matrigel (Corning). Two-hundred microlitres of cells mixed with matrigel were then loaded into a 1-ml insulin syringe (BD) and subcutaneously injected into the right back flank of an 8-week-old female BALB/c nude mouse. Rapamycin (LC Laboratories) in ethanol at 10 mg/ml was diluted in 5% Tween-80 (Sigma) and 5% PEG-400 (sigma). Treatment was conducted by intraperitoneal injection of 1.5 mg (low dose) or 4.5 mg (high dose) rapamycin every other day, starting at day 0 (the day of transplantation) or day 6. Xenografts were measured with a caliper every other day after transplantation (tumour volume = width^2 × length × 0.523). Tumour size must not exceed 20 mm at the largest diameter in an adult mouse, according to the IACUC and IRB of Beijing Laboratory Animal Research Center (BLARC). None of the experiments exceeded this limit in our study. Mice were killed when tumours reached 15 mm at the largest diameter or ulceration was evident. BALB/c nude mice were purchased from Charles River Laboratories and kept in a specific-pathogen-free facility at BLARC. Animals were maintained in accordance with institutional guidelines. We complied with all relevant ethical regulations of IACUA. Sample size was determined according to literatures. Mice were chosen in an unbiased fashion for experimental analysis to ensure randomization. The technicians who collected the data were blinded to genotype and treatment.

Patient samples. Breast cancer patient samples were all from Peking University Cancer Hospital, which owns a large breast cancer Biobank. Fresh breast tumour samples were obtained from patients and stored at −80 °C for further use. The tumours were all stage I–III. Tumour stage was classified according to the tumour-node-metastasis (TNM) classification of the Union International Cancer Control. This study was conducted in accordance with the ethics principles of the Declaration of Helsinki and approved by the Research and Ethics Committee of Peking University Cancer Hospital. All patients provided written informed consent.

Statistics and reproducibility. Unless otherwise stated, no statistical methods were used to predetermine sample size, the experiments were not randomized, and the investigators were not blinded to allocation during experiments and outcome assessment. The epidemiological data for association between transcript levels of KLHL22 and each cancer type, and the related statistical significances, were provided by the Oncomine platform. For graphs with error bars or statistical significance, details of reproducibility and statistics are indicated in the corresponding figure legends. All statistical analyses in our study were conducted using GraphPad Prism 5. For other graphs showing representative data, reproducibility are stated

below: (1) $n \geq 3$ biologically independent experiments for: Figs. 1a–j; 2a–e, g (statistical analysis in Extended Data Fig. 6f, h); 3a–e; 4a, d, e; Extended Data Figs. 1a, b (immunoblotting), c–f; 2a, d; 3b–e; 4a–d, f–h; 5a, b, d, f–h; 6b–d; 8a–c, e, g, h (immunoblotting), i; 9c–e. (2) $n = 3$ technically independent experiments for Fig. 4c. (3) $n = 1$ experiment for Extended Data Figs. 2b, c; 5e, i.
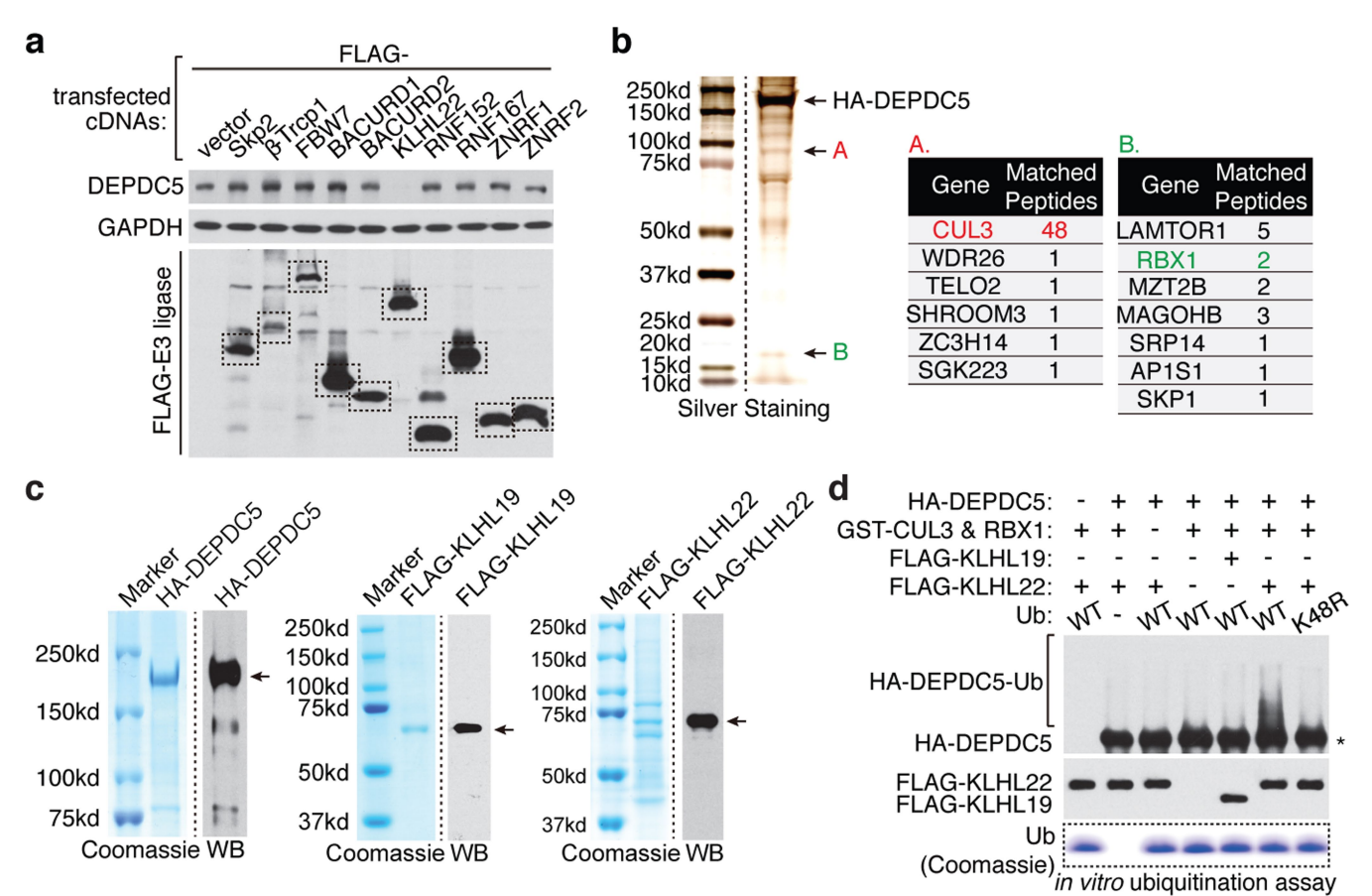
Reporting summary. Further information on experimental design is available in the Nature Research Reporting Summary linked to this paper.

Data availability. Source Data are available in the online version of the paper. The authors declare that all data supporting the findings of this study are available within the paper and its Supplementary Information files.
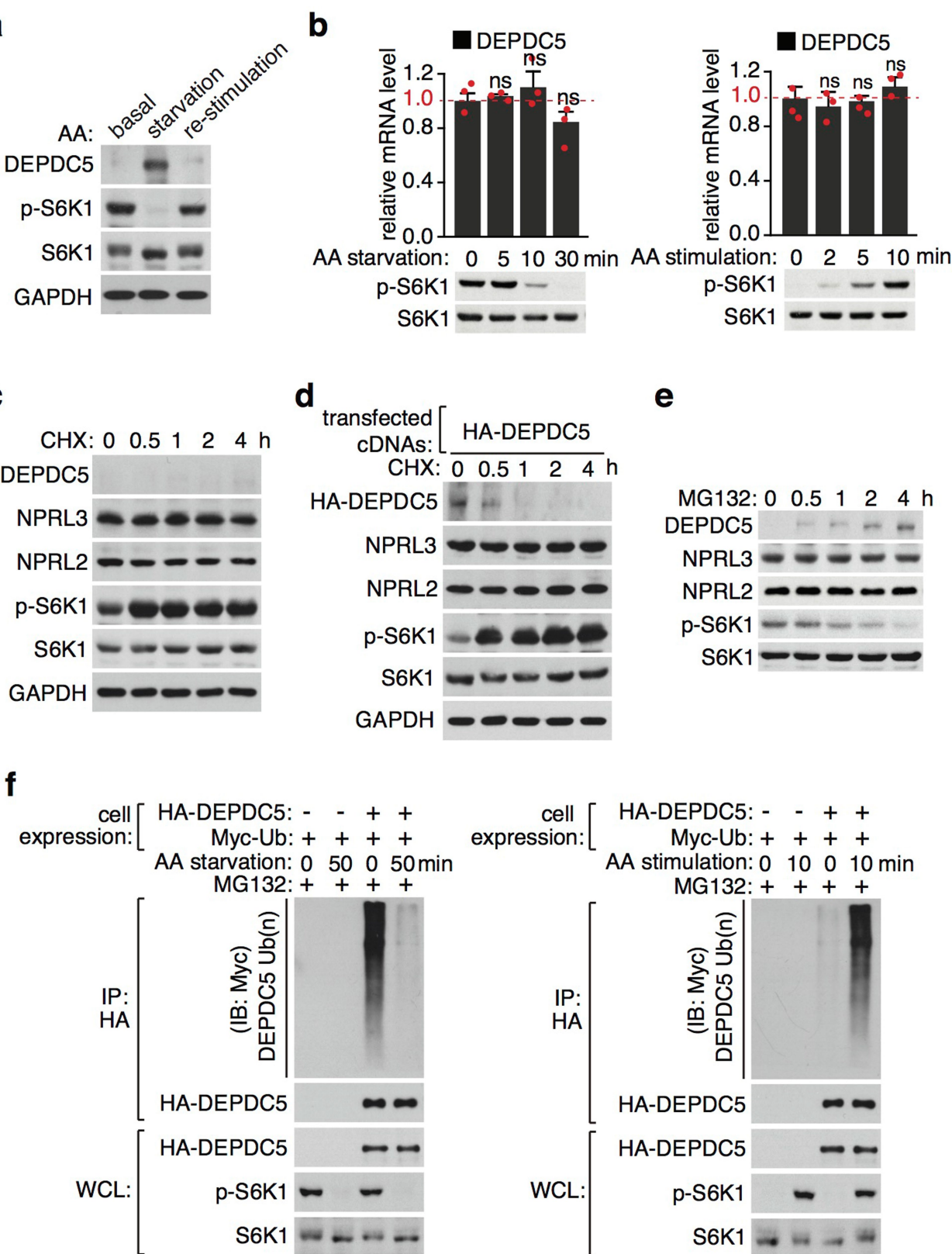
Extended Data Fig. 1 | DEPDC5 undergoes ubiquitin-mediated degradation in response to amino acids. a, Protein levels of endogenous DEPDC5 are regulated in response to the availability of amino acids. Basal, standard culture condition. **b**, Amino acids do not affect mRNA levels of DEPDC5. Relative mRNA levels of DEPDC5 to GAPDH were quantified by qPCR. $n = 3$ biologically independent experiments. ns, no significant difference; two-sided Student's t-test. **c, d**, DEPDC5 proteins are unstable under normal conditions. CHX, cycloheximide. **e**, Proteasome inhibitor MG132 increases the protein levels of DEPDC5. **f**, The ubiquitination of DEPDC5 is regulated in an amino-acid-dependent manner. For gel source data, see Supplementary Fig. 1.Source Data.

a

b

A.	
Gene	Matched Peptides
CUL3	48
WDR26	1
TELO2	1
SHROOM3	1
ZC3H14	1
SGK223	1

B.	
Gene	Matched Peptides
LAMTOR1	5
RBX1	2
MZT2B	2
MAGOHB	3
SRP14	1
AP1S1	1
SKP1	1

c

d

Extended Data Fig. 2 | CUL3–KLHL22 mediates the ubiquitination of DEPDC5. a, KLHL22, but not other E3 ligases, promotes the degradation of DEPDC5. **b**, DEPDC5 interacts with CUL3 and RBX1. Cells stably expressing HA–DEPDC5 were subjected to anti-HA immunoprecipitation. Arrows indicate protein bands on silver staining that were analysed by mass spectrometry. **c**, Purification of recombinant HA–DEPDC5, FLAG–KLHL19 or FLAG–KLHL22 proteins in HEK293T cells. **d**, CUL3–KLHL22 E3 ligase catalyses DEPDC5 ubiquitination in a cell-free system. Immunopurified HA–DEPDC5 and recombinant wild-type (WT) or mutant (K48R) ubiquitin were incubated with recombinant CUL3–RBX1 and KLHL22 or KLHL19. Asterisk represents HA–DEPDC5. For gel source data, see Supplementary Fig. 1.
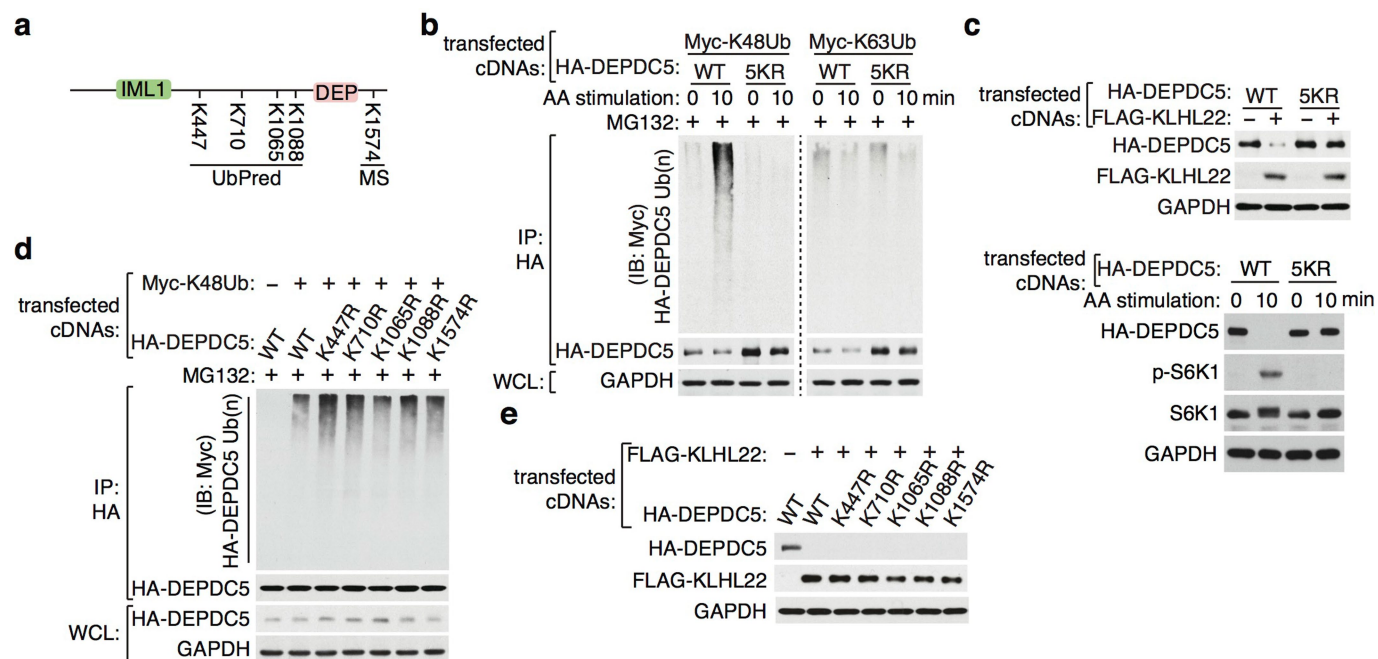
Extended Data Fig. 3 | KLHL22 promotes the ubiquitination of DEPDC5 on multiple lysine residues. a, Schematic depicting the predicted ubiquitination sites of DEPDC5. **b**, **c**, The 5KR mutation prevents K48-linked ubiquitination (**b**) and degradation (**c**) of DEPDC5. **d**, Single mutation of each lysine residue does not impair K48-linked ubiquitination (**d**) and degradation (**e**) of DEPDC5. For gel source data, see Supplementary Fig. 1.Source Data.
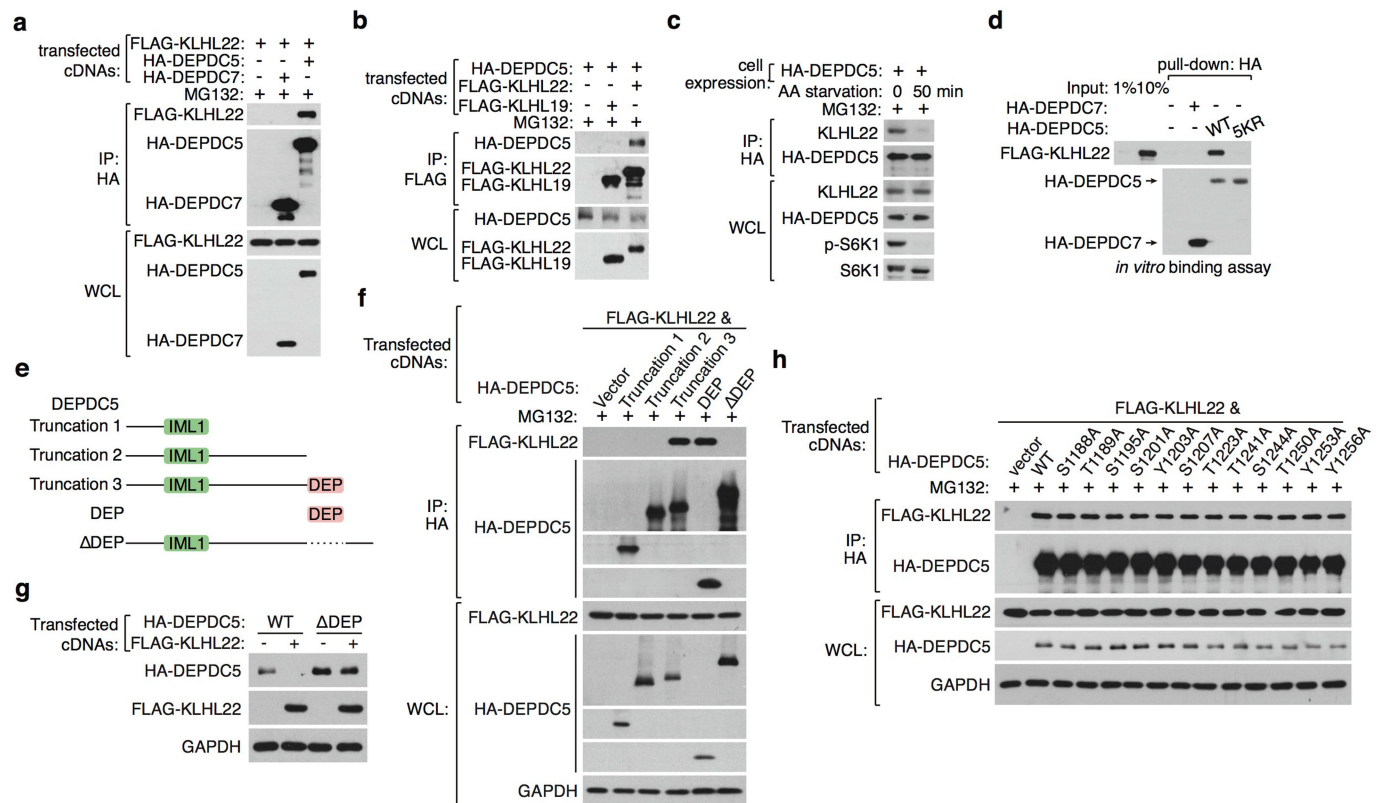
Extended Data Fig. 4 | DEP domain marks the degron of DEPDC5.
a, b, KLHL22 specifically interacts with DEPDC5. **c,** KLHL22 disassociates from DEPDC5 in response to amino acid starvation. **d,** Recombinant FLAG–KLHL22 directly interacts with WT but not 5KR HA–DEPDC5 in vitro. **e,** Schematic depicting the truncations of DEPDC5. **f,** KLHL22 interacts with DEPDC5 through the DEP domain. **g,** Deletion of DEP motif prevents KLHL22-mediated degradation of DEPDC5. **h,** Mutation of each serine, threonine or tyrosine residue in DEP domain to alanine does not affect the interaction between KLHL22 and DEPDC5. For gel source data, see Supplementary Fig. 1.
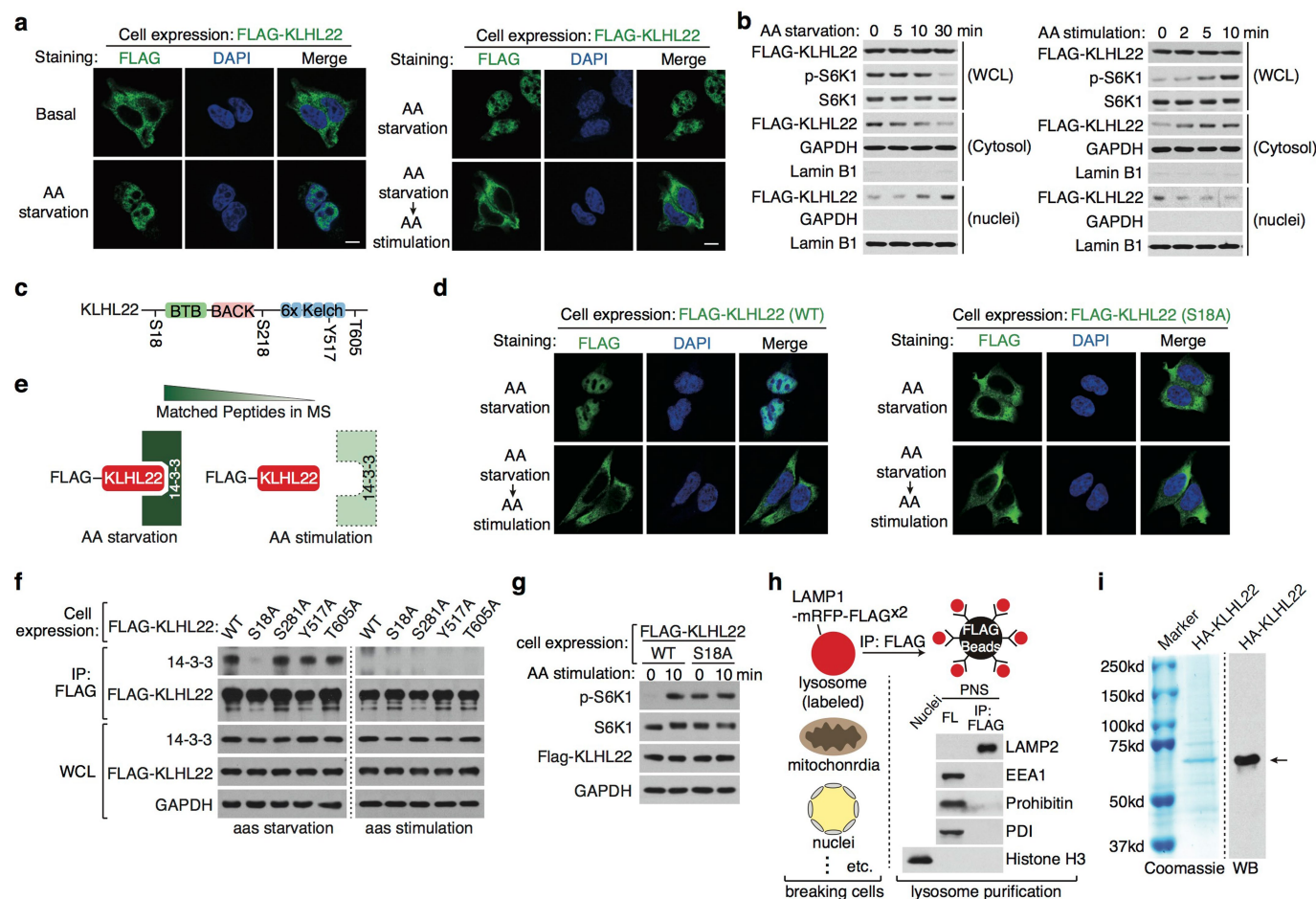
Extended Data Fig. 5 | 14–3–3 regulates nuclear–cytosolic shuttling of KLHL22. a, **b**, Nuclear–cytosolic shuttling of KLHL22 is regulated by amino acids. DAPI, nuclei. Scale bar, 10 μm. **c**, Schematic depicting the reported phosphorylation sites of KLHL22. **d**, S18A mutation prevents nuclear accumulation of KLHL22 in amino-acid-deficient conditions. Scale bar, 10 μm. **e**, Schematic depicting the interaction between FLAG–KLHL22 and 14-3-3 in mass spectrometry analysis using FLAG–KLHL22 as the bait. **f**, S18A mutation prevents the interaction between KLHL22 and 14-3-3 in amino-acid-deprived conditions. **g**, KLHL22(S18A) mutant promotes S6K1 phosphorylation in amino-acid-deficient conditions. **h**, Immunopurification of lysosomes. LAMP2 (lysosome), EEA1 (early endosome), prohibitin (mitochondria), PDI (endoplasmic reticulum) and histone H3 (nucleus). **i**, Purification of HA–KLHL22. For gel source data, see Supplementary Fig. 1.
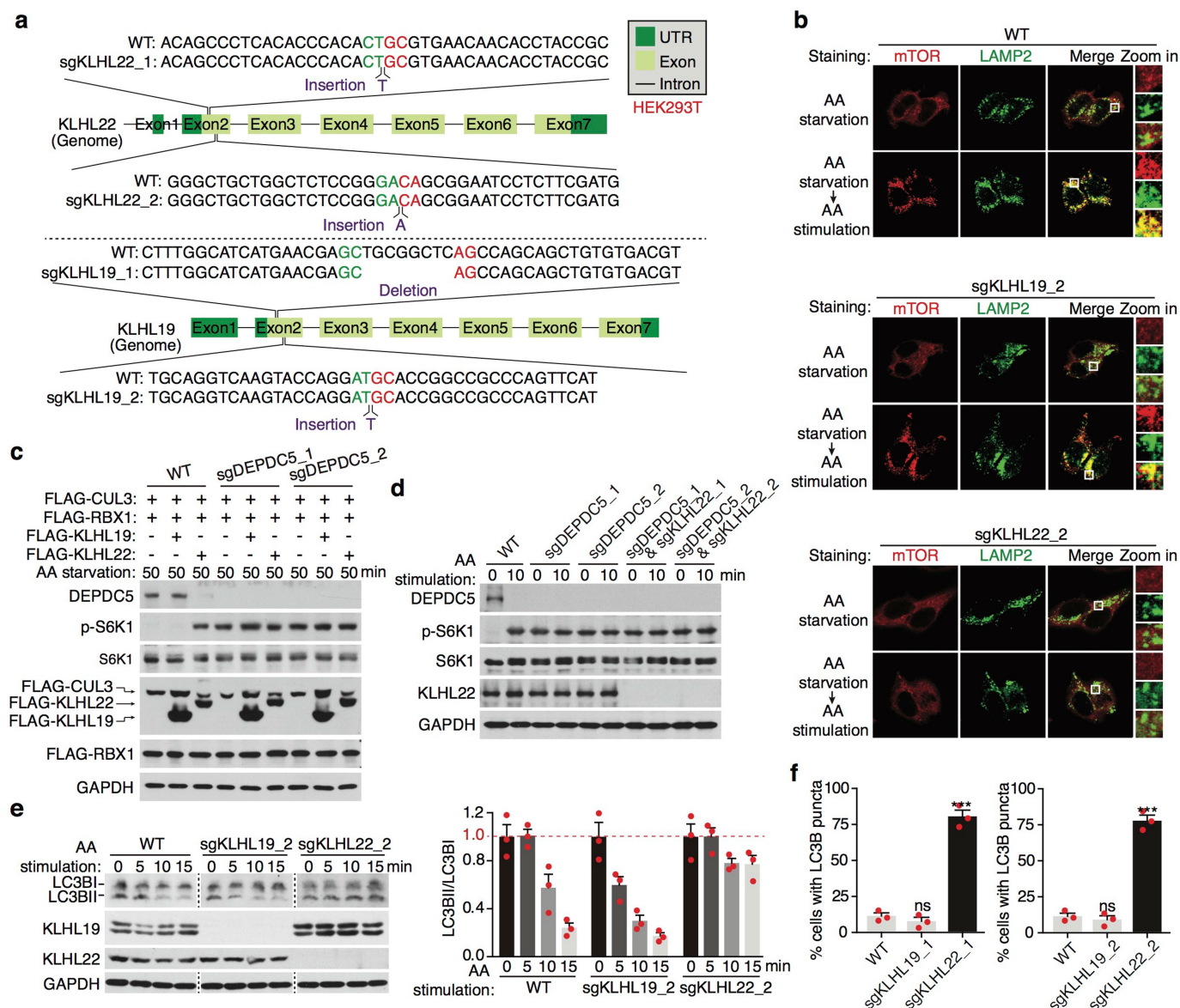
Extended Data Fig. 6 | KLHL22 is essential for activation of mTORC1 and downstream events. a, Schematic depicting CRISPR–Cas9-mediated knockout of *KLHL19* or *KLHL22* in HEK293T cells. **b**, KLHL22 is required for amino-acid-dependent lysosomal localization of mTORC1. Scale bar, 10 μm. **c**, **d**, Overexpression (**c**) or depletion (**d**) of KLHL22 does not affect mTORC1 activity in DEPDC5-deprived cells. **e**, KLHL22 is required for amino-acid-induced suppression of autophagy. $n = 3$ biologically independent experiments. **f**, Depletion of KLHL22 induces autophagy. Percentages of cells with obvious LC3B puncta were calculated. $n = 3$ biologically independent experiments. ns, no significant difference; ***$P < 0.001$; two-sided Student's *t*-test. For gel source data, see Supplementary Fig. 1.

a, Schematic depicting CRISPR–Cas9-mediated knockout of *KLHL19* or *KLHL22* in MEF cells. **b**, Predicted orthologues of KLHL22 in *C. elegans*. **c**, Knockdown efficiency of *tag-53*, *mel-26* and *T08A11.1*. $n = 2$ biologically independent experiments. **d**, RNAi targeting *T08A11.1*
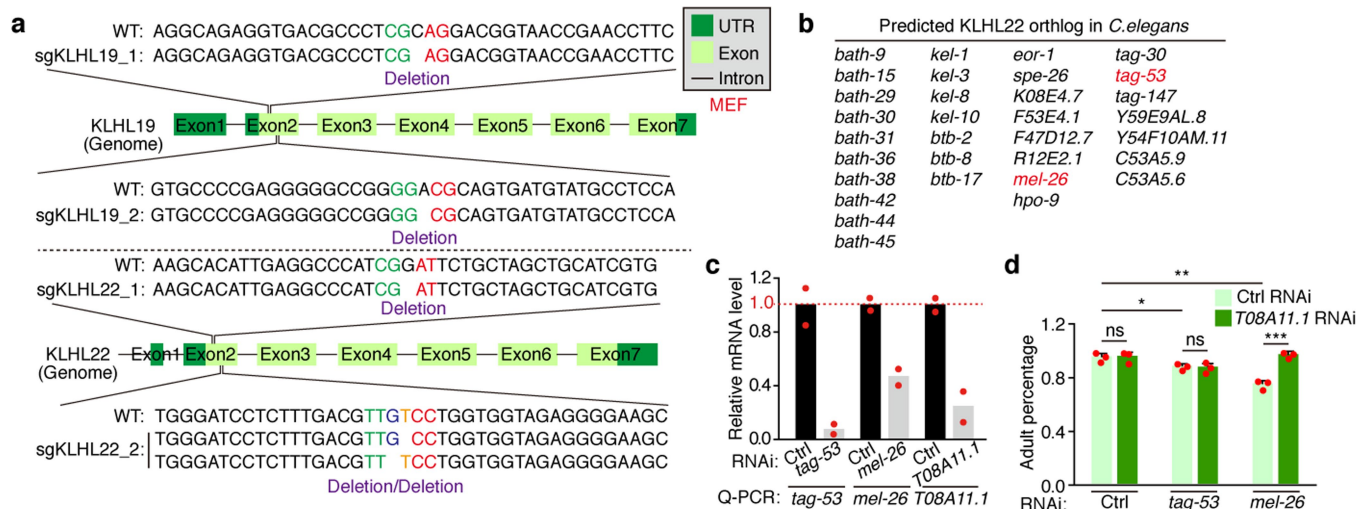
Extended Data Fig. 7 | KLHL22 has a conserved role in mice and nematodes.

suppresses the developmental delay of worms induced by *mel-26* RNAi, but not *tag-53* RNAi. $n = 3$ biologically independent experiments. ns, no significant difference; $*P < 0.05$; $**P < 0.01$; $***P < 0.001$; two-sided Student's *t*-test.
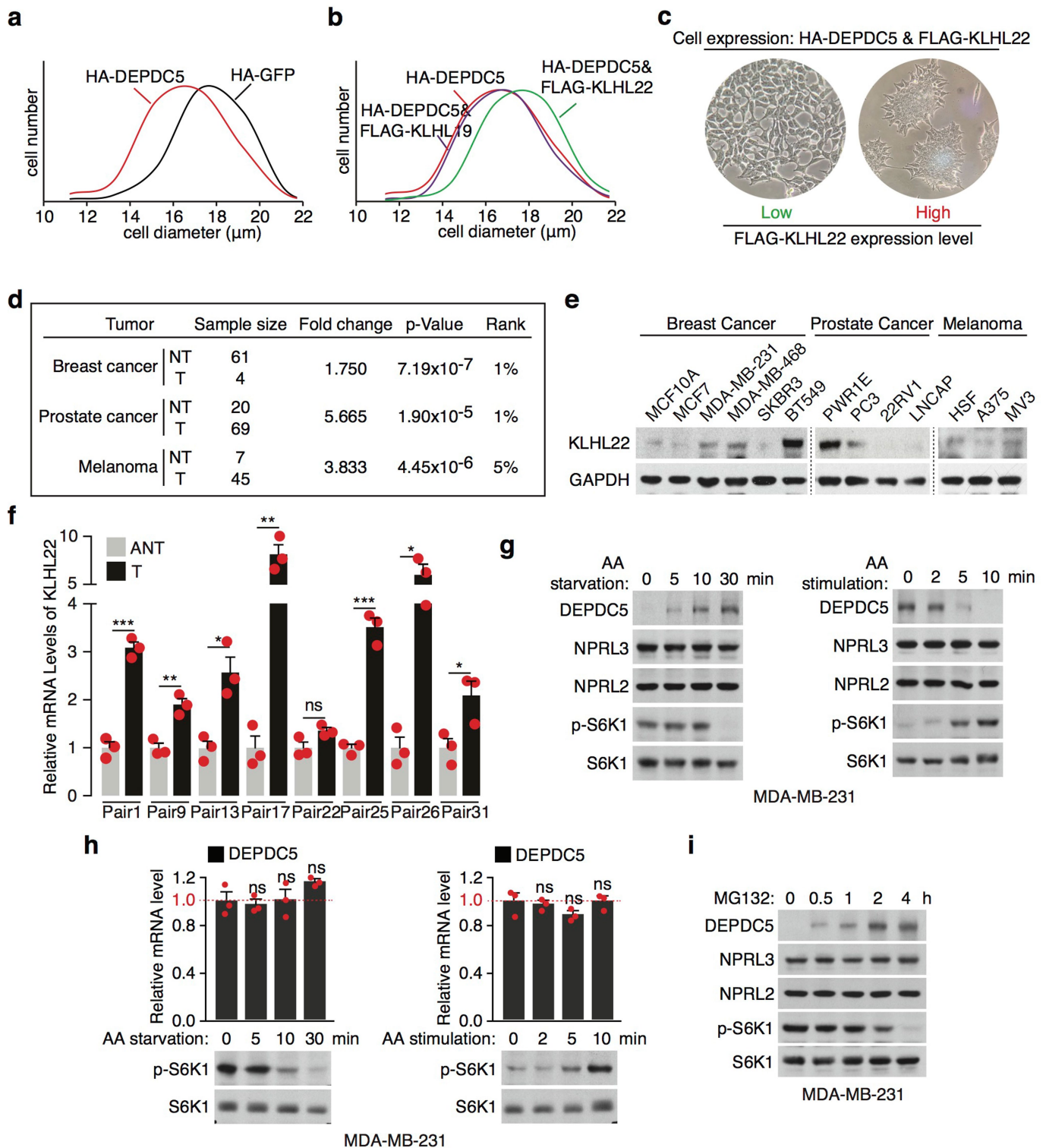
Extended Data Fig. 8 | Protein levels of KLHL22 are elevated in human breast cancer. a, Stable expression of HA–DEPDC5 reduces the size of HEK293T cells. **b**, Stable expression of FLAG–KLHL22 reverses the reduction in cell size in HEK293T cells stably expressing HA–DEPDC5. **c**, High expression of FLAG–KLHL22 transforms HEK293T cells. **d**, According to Oncomine database, mRNA levels of KLHL22 are elevated in breast and prostate cancers and in melanoma. Fold change of KLHL22 transcript levels in tumour tissues (T) to the corresponding normal tissues (NT) are shown. Rank represents KLHL22 rank in ordered list of genes that are upregulated. **e**, Protein levels of KLHL22 in breast cancer, prostate cancer and melanoma cell lines and corresponding normal cells (MAF10A, PWR1E and HSF). **f**, mRNA levels of KLHL22

are elevated in tumours of breast cancer patients. T: tumours; ANT: adjacent normal tissues. Quantifications are normalized to actin. $n = 3$ technically independent experiments. ns, no significant difference; $*P < 0.05$; $**P < 0.01$; $***P < 0.001$; two-sided Student's t-test. **g**, Protein levels of endogenous DEPDC5 are regulated in an amino-acid-sensitive manner in MDA-MB-231 cells. **h**, Amino acid deprivation or stimulation does not affect mRNA levels of DEPDC5 in MDA-MB-231 cells. Relative mRNA levels of DEPDC5 to GAPDH were quantified using qPCR. $n = 3$ biologically independent experiments. ns, no significant difference; two-sided Student's t-test. **i**, Proteasome inhibitor MG132 increases the protein levels of DEPDC5 in MDA-MB-231 cells. For gel source data, see Supplementary Fig. 1.
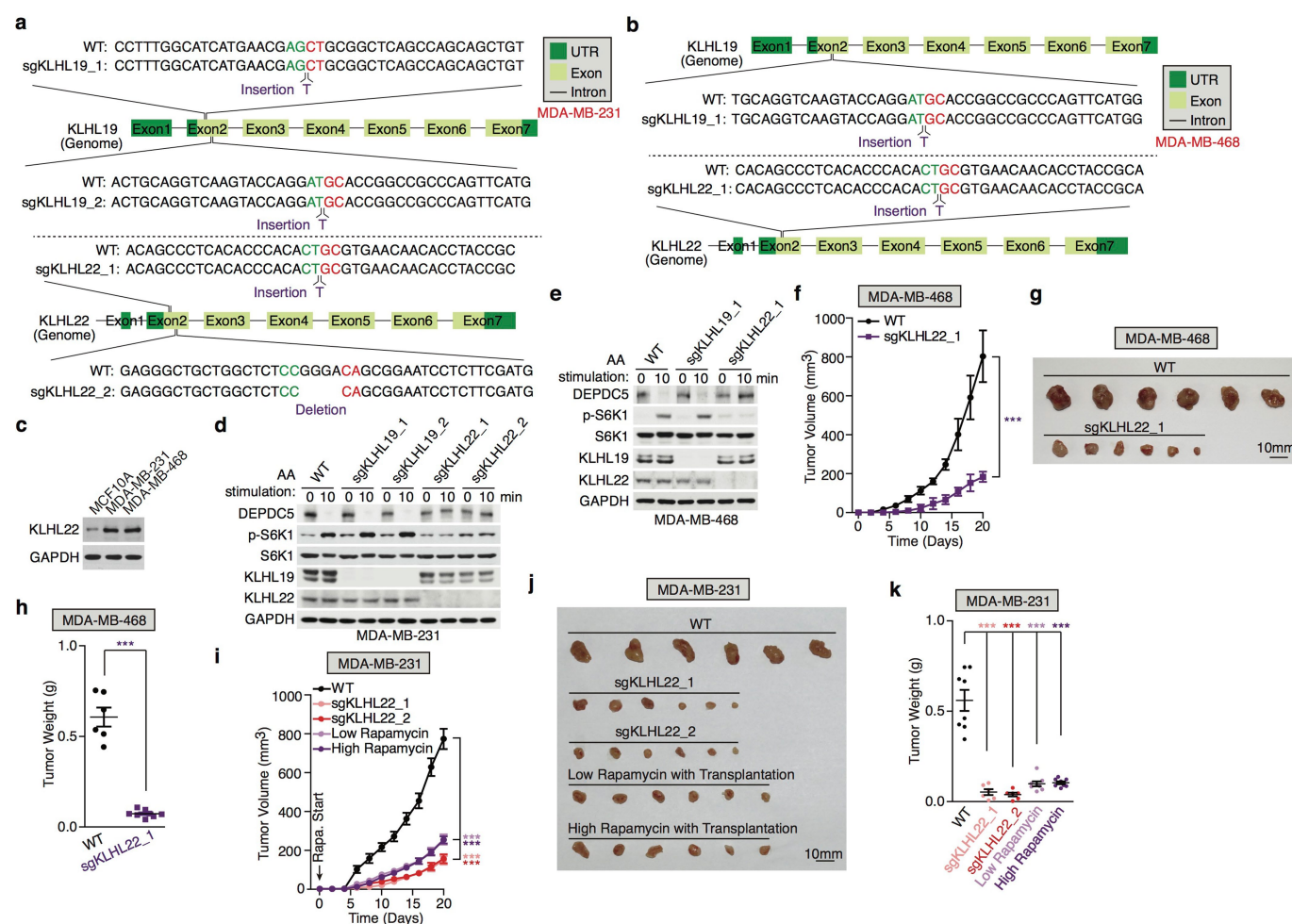
Extended Data Fig. 9 | Deletion of KLHL22 in breast cancer cells prevents mTORC1 activation and tumorigenesis. a, **b**, Schematic of CRISPR–Cas9-mediated knockout of *KLHL19* or *KLHL22* in MDA-MB-231 (**a**) or MDA-MB-468 (**b**) breast cancer cells. **c**, Protein levels of KLHL22 are upregulated in MDA-MB-231/468 cells. **d**, **e**, Deletion of KLHL22 in MDA-MB-231 (**d**) or MDA-MB-468 (**e**) cells suppresses amino-acid-induced DEPDC5 degradation and S6K1 phosphorylation. **f**–**h**, Deletion of KLHL22 suppresses tumour growth of MDA-MB-468 cells. Tumour volume, mean ± s.e.m. ($n = 9$ mice for WT, $n = 8$ mice for sgKLHL22_1), ***$P < 0.001$, two-sided ANOVA (**f**); tumour images (**g**); tumour weights 20 days after transplantation,

mean ± s.e.m. ($n = 6$ mice for WT and $n = 8$ mice for KLHL22 knockouts), ***$P < 0.001$, two-sided Student's *t*-test (**h**). **i**–**k**, Deletion of KLHL22 or treatment with rapamycin suppresses tumour growth of MDA-MB-231 cells. Tumour volume, mean ± s.e.m. ($n = 9$ mice for sgKLHL22_2 and WT injected with low dose of rapamycin, $n = 10$ mice for remaining groups), ***$P < 0.001$, two-sided ANOVA (**i**); tumour images (**j**); and tumour weights 20 days after transplantation, mean ± s.e.m. ($n = 8$ mice for WT and WT injected with low or high dose of rapamycin; $n = 6$ mice for KLHL22 knockouts), ***$P < 0.001$, two-sided Student's *t*-test (**k**). For gel source data, see Supplementary Fig. 1.Source Data.
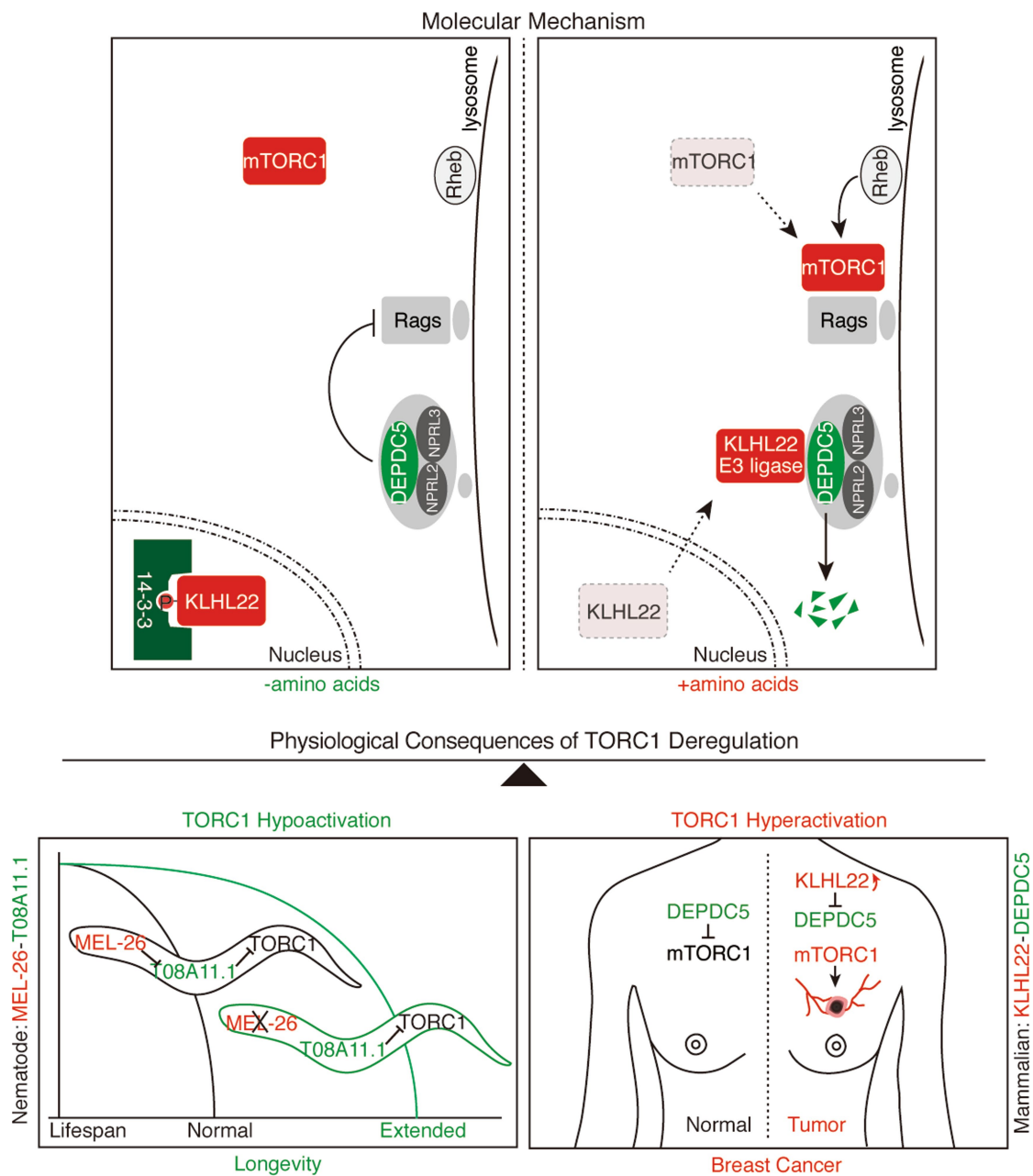
Extended Data Fig. 10 | Proposed model of KLHL22-mediated regulation of mTORC1, ageing and cancer. In response to amino acids, KLHL22 translocates from the nucleus to the cytosol, where it accumulates on the surface of lysosomes to mediate the ubiquitination and degradation of DEPDC5, an essential subunit of GATOR1. GATOR1 loss of function activates Rag GTPases and subsequently activates mTORC1 (top). KLHL22-mediated DEPDC5 degradation is a conserved mechanism of TORC1 regulation in mammals and nematode. TORC1 hypoactivation due to *mel-26* (*Ce*.KLHL22) depletion extends *C. elegans* lifespan, whereas TORC1 hyperactivation due to elevated expression of KLHL22 promotes human breast cancer (bottom).

naturereseach

Corresponding author(s):   Ying Liu

Reporting Summary

Nature Research wishes to improve the reproducibility of the work that we publish. This form provides structure for consistency and transparency in reporting. For further information on Nature Research policies, see [Authors & Referees](#) and the [Editorial Policy Checklist](#).

Statistical parameters

When statistical analyses are reported, confirm that the following items are present in the relevant location (e.g. figure legend, table legend, main text, or Methods section).

n/a	Confirmed	
☐	☒	The exact sample size (*n*) for each experimental group/condition, given as a discrete number and unit of measurement
☐	☒	An indication of whether measurements were taken from distinct samples or whether the same sample was measured repeatedly
☐	☒	The statistical test(s) used AND whether they are one- or two-sided *Only common tests should be described solely by name; describe more complex techniques in the Methods section.*
☐	☒	A description of all covariates tested
☒	☐	A description of any assumptions or corrections, such as tests of normality and adjustment for multiple comparisons
☐	☒	A full description of the statistics including central tendency (e.g. means) or other basic estimates (e.g. regression coefficient) AND variation (e.g. standard deviation) or associated estimates of uncertainty (e.g. confidence intervals)
☐	☒	For null hypothesis testing, the test statistic (e.g. F, t, r) with confidence intervals, effect sizes, degrees of freedom and P value noted *Give P values as exact values whenever suitable.*
☒	☐	For Bayesian analysis, information on the choice of priors and Markov chain Monte Carlo settings
☒	☐	For hierarchical and complex designs, identification of the appropriate level for tests and full reporting of outcomes
☒	☐	Estimates of effect sizes (e.g. Cohen's *d*, Pearson's *r*), indicating how they were calculated
☐	☒	Clearly defined error bars *State explicitly what error bars represent (e.g. SD, SE, CI)*

Our web collection on [statistics for biologists](#) may be useful.

Software and code

Policy information about [availability of computer code](#)

Data collection	No software was used.
Data analysis	GraphPad Prism 5.0 for statistics; ImageJ 1.48v for image analysis; C. elegans Codon Adaptor for codon optimization; UbPred for ubiquitination sites prediction; Optimized CRISPR Design for designing CRISPR gRNAs.

For manuscripts utilizing custom algorithms or software that are central to the research but not yet described in published literature, software must be made available to editors/reviewers upon request. We strongly encourage code deposition in a community repository (e.g. GitHub). See the Nature Research [guidelines for submitting code & software](#) for further information.

Data

Policy information about [availability of data](#)

All manuscripts must include a [data availability statement](#). This statement should provide the following information, where applicable:

- Accession codes, unique identifiers, or web links for publicly available datasets
- A list of figures that have associated raw data
- A description of any restrictions on data availability

The authors declare that all data supporting the findings of this study are available within the paper and the Supplementary Information files.

Field-specific reporting

Please select the best fit for your research. If you are not sure, read the appropriate sections before making your selection.

☒ Life sciences   ☐ Behavioural & social sciences

For a reference copy of the document with all sections, see nature.com/authors/policies/ReportingSummary-flat.pdf

Life sciences

Study design

All studies must disclose on these points even when the disclosure is negative.

Sample size	(1) For all immunoblotting, immunostaining, Q-PCR, size determination and clone formation related experiments using cells (Figure 1a-i, 2a-h, 3a-b, 4a-b, 4d-e; Extended Figure 1a-f, 2a, 3b-e, 4a-c, 4f-h, 5a-b, 5d, 5f-g, 6b-f, 8a-c, 8e, 8g-i, 9c-e), sample size is not determined because there are million of cells per sample and it is unnecessary to pre-determine the number of cells. The representative data of n>=3 biological replicates with similar results are displayed. (2) For all "in vitro" experiments using purified proteins (Figure 1j; Extended Figure 2d, 4d, 5h), sample size is not determined because there are countless proteins per sample and it is unnecessary to pre-determine the number of proteins. The representative data of n>=3 biological replicates with similar results are displayed. (3) For the mass spectrometry assays using cells (Extended Figure 2b, 5e), sample size is determined according to literatures using 5 x 15cm dishes of cells (around 200 million cells). Mass spectrometry experiments are not repeated. (4) For HLH-30 nuclear localization in worm (Figure 3c-e), sample size is determined according to our pretested results and our previously published paper (PMID: 29027899). n>=40 worms per sample. (5) For Q-PCR of worm genes (Extended Figure 7c), sample size is determined according to our pretested results and our previously published paper (PMID: 29027899). n=300 (around) worms per sample. (6) For worm growth study (Extended Figure 7d), sample size is determined according to our pretested results. n=100 (around) worms per sample. (7) For lifespan analysis (Figure 3f-g), sample size is determined according to our pretested results, our previously published paper (PMID: 29027899) and related analysis in literatures. n=100 (around) worms per sample. (8) For immunoblotting and Q-PCR experiments using human samples (Figure 4c; Extended Figure 8f), sample size is limited by the patient samples that we could obtain and is indicated in Figure legends. (9) For tumor growth experiments using naked mice (Figure 4f, 4h; Extended Figure 9f, 9h-i, 9k), sample size is determined according to the related analysis in literature (PMID: 27912060) and is indicated in Figure legends.
Data exclusions	For lifespan assays, worms that crawled off the plate or underwent vulva blasting could cause irregular death and were not included in the data. This exclusion criteria has been established and extensively used in the field.
Replication	(1) For mass spectrometry assays, no biological replication was conducted. (2) The rest of experiments were repeated and our data are based on at least two to three independent experiments with similar results. Details are described at the end of methods part entitled "Statistics and Reproducibility".
Randomization	For lifespan analysis, worms were raised on plates, and they were chosen unbiasedly for experimental analysis to ensure randomization. For tumor growth, mice of similar ages were randomly allocated into different groups.
Blinding	(1) For all immunoblotting, siver staining and Q-PCR related experiments (Figue 1a-h, 1j, 2b-c, 2e-f, 3b, 4a, 4c; Extended Figure 1a-f, 2a-d, 3b-e, 4a-c, 4f-h, 5b, 5e-i, 6c-e, 7c, 8e-i, 9c-e), no blinding was used during data collection because data from different groups were generated simultaneously, no personal bias will be involved. (2) For all imaging related experiments (Figure 1i, 2a, 2d, 2g, 3a, 3c-e; Extended Figure 5a, 5d, 6b, 6f, 8c,), data from different groups were unbiasedly collected and were double checked by Jie Chen and Yuhui Ou. So no blinding was used. (3) For C. elegans lifespan analysis (Figure 3f-g), C. elegans growth analysis (Extended Figure 7d) and tumor growth experiments (Figure 4f-h, 9f-k), the technicians who collected the data were blind to the genotypes and treatments. (4) For cell diameter determination (Figure 2h; Extended Figure 8a-b) and clone formation assays (Figure 4b, 4d-e), data are directly collected and analyzed by machines and there is no personal bias during data collection.

Materials & experimental systems

Policy information about availability of materials

n/a	Involved in the study
☒	☐ Unique materials
☐	☒ Antibodies
☐	☒ Eukaryotic cell lines
☐	☒ Research animals
☐	☒ Human research participants

Antibodies

Antibodies used	(1) Mouse monoclonal anti-HA: Supplier/Santa Cruze; Cat.No./7392; Lot.No./C0816; CloneName/F-7; Dilution/1:250; Supplier's statement/Westen blot analysis of HA-tagged fusion protein showing N-terminal HA-tagged JNK2, JNK1 and C-terminal HA-

tagged Daxx; Citation[PMID]/11161216; Main figures in this paper/Figure 1b-c, 1h, 1j, 2c.

(2) Rabbit polyclonal anti-Flag: Supplier/Sigma; Cat.No./F7425; Lot.No./064M4757V; CloneName/NA; Dilution/1:1000 (immunoblotting), 1:100 (immunostaining); Supplier's statement/For immunoblotting, a minimum working concentration of 1-2.5ug/ml detects N-terminal FLAG-BAP fusion protein in an E. coli crude cell lysate and 1 ng of N-terminal FLAG-BAP fusion protein spiked in COS-7 whole cell extract. For immunostaining, a minimum working concentration of 5- 10ug/ml detects FLAG fusion protein in methanol-acetone fixed transiently transfected cells; Citation[PMID]/8770418; Main figures in this paper/Figure 1d-e, 1i-j, 2c-d, 4a.

(3) Mouse monoclonal anti-LAMP2: Supplier/Abcam; Cat.No./25631; Lot.No./GR216989-1; CloneName/H4B4; Dilution/1:1000 (immunoblotting), 1:100 (immunostaining); Supplier's statement/For immunoblotting, The antibody works really good on human samples, detecting a single 110 kDa band but it's not suitable to use for mouse or rat samples. For immunoblotting, ab25631 staining LAMP2 in human THP-1 cells. Citation[PMID]/28195531; Main figures in this paper/Figure 1i, 2a.

(4) Rat monoclonal anti-LAMP2: Supplier/Abcam; Cat.No./13524; Lot.No./Lost; CloneName/GL2A7; Dilution/1:100 (immublotting); Supplier's statement/For immunostaining, LAMP2 stains lysosomes in adult mouse cardiac myocytes using the dilution of 1/100; Citation[PMID]/28589926; Main figures in this paper/Figure 3a.

(5) Rabbit monoclonal anti-EEA1: Supplier/CST; Cat.No./3288; Lot.No./04/2015-7; CloneName/C45B10; Dilution/1:1000; Supplier's statement/Western blot analysis of extracts from various cell lines using EEA1 (C45B10) Rabbit mAb; Citation[PMID]/10050856. Data in this paper/Extended Figure 5h.

(6) Rabbit monoclonal anti-GAPDH: Supplier/Abcam; Cat.No./128915; Lot.No./GR90965-16; CloneName/EPR6256; Dilution/1:10000; Supplier's statement/Lysate of 293T, HeLa, HepG2, HUVEC, MCF7 and SHSY5Y are analyzed using GAPDH anti body at 1:1000 dilution; Citation[PMID]/28877997; Main figures in this paper/Figure 1c-d, 1f-g, 2b-c, 2e-f, 4a.

(7) Mouse monoclonal anti-Lamin B1: Supplier/Bioworld; Cat.No./MB2029; Lot.No./CH36131; Dilution/1:1000; Supplier's statement/Lamin B1 mAb detects endogenous levels of Lamin B1 protein in HepG2 and 293T cell lysates. Data in this paper/ Extended Figure 5b.

(8) Mouse monoclonal anti-Histone H3: Supplier/CST; Cat.No./3638; Lot.No./Lost; Dilution/1:1000; Supplier's statement/ Western blots of extracts from HeLa, NIH/3T3, C6 and COS cell lines using Histone H3 (96C10) are validated. Citation[PMID]/29162813; Data in this paper/Extended Figure 5h.

(9) Mouse monoclonal anti-Actin: Supplier/Sigma; Cat.No./A5441; Lot.No./064M4789V; Dilution/1:10000; Supplier's statement/ Western blots of HeLa, JURKAT, COS7, NIH-3T3, PC-12, RAT2, CHO, MDBK and MDCK cell lines are validated; Citation[PMID]/NA; Main figures in this paper/Figure 4c.

(10) Mouse monoclonal anti-14-3-3: Supplier/Santa Cruze; Cat.No./23957; Lot.No./I2216; Dilution/1:250; Western blot analysis of 14-3-3ε expression in HeLa, SK-N-SH, NIH/3T3, C4, C6 and A-10 whole cell lysates are validated. Data in this paper/Extended Figure 5f.

(11) Rabbit monoclonal anti-PDI: Supplier/Santa Cruze; Cat.No./20132; Lot.No./G0715; CloneName/C45B10; Dilution/1:250; Supplier's statement/Western blot analysis of PDI in 293T is validated; Citation[PMID]/18319612. Data in this paper/Extended Figure 5h.

(12) Rabbit polyclonal anti-Prohibitin: Supplier/Santa Cruze; Cat.No./28259; Lot.No./F0515; CloneName/H-80; Dilution/1:250; Supplier's statement/Western blot analysis of Prohibitin in A-431 and Ramos are validated; Citation[PMID]/25240327. Data in this paper/Extended Figure 5h.

(13) Rabbit polyclonal anti-NPRL2: Supplier/Sigma; Cat.No./SAB1305758; Lot.No./SA111109AN; Dilution/1:1000; Supplier's statement/Western blot analysis in HL-60 cell line lysate is validated; Citation[PMID]/NA; Main figures in this paper/Figure 1a-b, 1e.

(14) Rabbit polyclonal anti-NPRL3: Supplier/Sigma; Cat.No./HPA011741; Lot.No./A96412; Dilution/1:250; Supplier's statement/ Immunofluorescent staining of human cell line A-431 shows positivity in cytoplasm; Citation[PMID]/28199315; Main figures in this paper/Figure 1a-b, 1e.

(15) Rabbit polyclonal anti-DEPDC5: Supplier/Sigma; Cat.No./SAB1302644; Lot.No./1643-1002; Dilution/1:250; Supplier's statement/Western blot analysis in K562 cell line lysate is validated; Citation[PMID]/NA; Main figures in this paper/Figure 1a-b, 1d-g, 2b, 3b, 4c.

(16) Rabbit polyclonal anti-p-S6K1: Supplier/CST; Cat.No./9205; Lot.No./06/2017-16; Dilution/1:1000; Supplier's statement/ Western blot analysis of HeLa, COS, C6 and 3T3 cells has been validated; Citation[PMID]/ 29079776; Main figures in this paper/ Figure 1a-b, 1h, 2b-c, 2e, 3b.

(17) Rabbit polyclonal anti-S6K1: Supplier/CST; Cat.No./9202; Lot.No./03/2016-20; Dilution/1:1000; Supplier's statement/ Western blot analysis of extracts from HeLa, NIH-3T3, PC12 and COS-7 cells are validated; Citation[PMID]/ 29259156; Main figures in this paper/Figure 1a-b, 1h, 2b-c, 2e, 3b.

(18) Rabbit monoclonal anti-mTOR: Supplier/Cell Signaling; Cat.No./2983; Lot.No./01/2015-14; CloneName/7C10; Dilution/1:100 (immunostaining); Supplier's statement/Immunostaining analysis of MEF cells has been validated; Citation[PMID]/29153837; Main figures in this paper/Figure 2a, 3a.

(19) Rabbit polyclonal anti-LC3B: Supplier/Sigma; Cat.No./L7543; Lot.No./17-03-08-032; CloneName/NA; Dilution/1:100; Supplier's statement/Immunostaining analysis of HeLa cells has been validated; Citation[PMID]/24089213; Main figures in this paper/Figure 2g.

(20) Rabbit polyclonal anti-Myc: Supplier/ImmunoWay; Cat.No./YM3203; Lot No./B0301; CloneName/NA; Dilution/1:5000; Supplier's statement/1ug C-Myc fusion protein with Primary antibody dilution at 1:5000 is sufficient to be seen; Citation[PMID]/ NA; Main figures in this paper/Figure 1c, 2c.

(21) Mouse monoclonal anti-Ub: Supplier/Santa Curz; Cat.No./8017; Lot No./K2014; CloneName/P4D1; Dilution/1:250; Supplier's statement/Western blot analysis of Ub in 293T cell lysate is validated; Citation[PMID]/ 29107329; Main figures in this paper/ Figure 1d, 1f.

(22) Rabbit Polyclonal anti-KLHL22: Supplier/Proteintech; Cat.No./16214-1-AP; Lot No./NA; CloneName/NA; Dilution/1:1000; Supplier's statement/Western blot analysis of human brain tissue has been validated; Citation[PMID]/26323689; Main figures in this paper/Figure 1f-h, 2b, 2e-f, 3b, 4c.

(23) Rabbit Polyclonal anti-KLHL19: Supplier/Proteintech; Cat.No./10503-2-AP; Lot No./NA; CloneName/NA; Dilution/1:1000; Supplier's statement/WB result in HEK293 cells is validated; Citation[PMID]/29230017; Main figures in this paper/Figure 1f, 2b, 2f, 3b.

Validation	Validations of the antibodies are indicated above.

Eukaryotic cell lines

Policy information about [cell lines](#)

Cell line source(s)	HEK293T cell was purchased from ATCC. MCF10A, MCF7, SKBR3, BT549, PWR1E, 22RV1, LNCAP and HSF cells were provided by Dr. Gaoliang Ouyang (Xiamen University); A375 and MV3 cells were provided by Dr. Qiao Wu (Xiamen University); MDA-MD-231, MDA-MB-468, PC3 and MEF cells were gifts from Dr. Sheng-Cai Lin (Xiamen University).
Authentication	Cell lines served in this study were not authenticated right before usage.
Mycoplasma contamination	All cell lines were validated to be free of mycoplasma contamination.
Commonly misidentified lines (See [ICLAC](#) register)	No commonly misidentified cell lines were used.

Research animals

Policy information about [studies involving animals](#); [ARRIVE guidelines](#) recommended for reporting animal research

Animals/animal-derived materials	C. elegans strains (N2; EU1007: mel-26; MAH240: HLH-30::GFP) were obtained from the Caenorhabditis Genetics Center (CGC). 8-week old female BALB/c nude mice (around 15g/mouse) were from Charles River Laboratories and kept in a specific-pathogen-free facility at Beijing Laboratory Animal Research Center (BLARC). Mouse-related experiments were conducted in accordance with institutional guidelines.

Human research participants

Policy information about [studies involving human research participants](#)

Population characteristics	Fresh breast tumor samples were obtained from woman patients and stored at -80°C for further use. The tumors are all stage I to stage III. Tumor stage was classified according to the tumor-node-metastasis (TNM) classification of the Union International Cancer Control. This study was conducted in accordance with the ethics principles of the Declaration of Helsinki and approved by the Research and Ethics Committee of Peking University Cancer Hospital. All patients provided written informed consent.

Method-specific reporting

n/a	Involved in the study
☒ ☐	ChIP-seq
☒ ☐	Flow cytometry
☒ ☐	Magnetic resonance imaging